Nanoscale Advances

ROYAL SOCIETY OF CHEMISTRY

PAPER

View Article Online
View Journal | View Issue

Cite this: *Nanoscale Adv.*, 2025, **7**, 5735

Evaluation of the safety profile of a metal-based nanosystem for developing antimicrobial polymer membranes in healthcare applications†

Piumika Yapa, [a] Imalka Munaweera *[a] and Mayuri Geethanjalie Thammitiyagodage *[b]

Healthcare-associated infections remain a significant concern, driving the exploration of metal-based nanosystems as innovative solutions for developing antimicrobial polymer membranes. This study evaluates the toxicity of a novel nanofiber membrane reinforced with multimetallic silica nanohybrids, proposed as an advanced antimicrobial layer. Initially, silver (Ag), copper (Cu), and cobalt (Co) were doped into silica nanoparticles (SiNPs) *via* the sol–gel method. The trimetallic nanohybrid demonstrated superior antimicrobial activity compared to Ag-, Cu-, or Co-doped SiNPs alone, showing enhanced efficacy against Gram-positive and Gram-negative bacteria, as well as fungi, due to the synergistic action of the metals. Toxicity was assessed using zebrafish embryo assays (OECD 236) with concentrations ranging from 10.000 to 0.156 mg L^{-1}. LC_{50} values were 2.05 mg L^{-1} (AgSiNPs), 5.53 mg L^{-1} (CuSiNPs), 9.99 mg L^{-1} (CoSiNPs), and 6.35 mg L^{-1} (trimetallic SiNPs). Based on these results, the trimetallic nanohybrid, which showed the lowest toxicity, was electrospun into a polymer membrane. Skin irritation was evaluated using the HET-CAM assay (ICCVAM protocol), yielding irritation scores of 13.33 ± 0.58 (Ag), 11.67 ± 0.58 (Cu), 1.00 ± 1.00 (Co), and 3.67 ± 0.58 (trimetallic), suggesting minimal irritation potential ($p = 0.05$). Franz diffusion cell analysis detected no Cu or Co, and only 0.26 mg L^{-1} of Ag after 24 hours, well below toxic thresholds. Statistical analysis ($p < 0.05$) confirmed the safety of the membrane, showing reduced toxicity and minimal metal nanohybrid diffusion. The multimetallic nanohybrid membrane is therefore considered safe as an antimicrobial polymer membrane in healthcare applications and recommends further *in vivo* evaluation.

Received 19th April 2025
Accepted 23rd July 2025

DOI: 10.1039/d5na00380f

rsc.li/nanoscale-advances

1 Introduction

In recent years, the field of nanotechnology has experienced remarkable advancements, revolutionizing various sectors, particularly biomedicine and materials science. The implication of nanoparticles in the delivery of healthcare might be the enhancement of the positive effects of treatment and the reduction of the negative effects, and overall, the experience of the patient can be enhanced.[1] It is crucial to identify how nanotechnology has transformed the field of biomedical science, especially in relation to the crises of antimicrobial resistance (AMR). Metallic nanoparticles, especially metal-based nanosystems, have been of considerable interest for their unique properties and potential use in developing antimicrobial polymer membranes in healthcare.[2,3] More recently, the WHO sounded the 'emergency call,' in response to which they estimated that by 2050, AMR could result in 10 million annual fatalities. This proves the necessity of the broad-spectrum antimicrobial agents, which are not seen as a part of resistance.[4]

Metallic nanoparticles have been positively associated with antimicrobial properties, whereby such particles exert their actions through mechanisms including the production of ROS radicals, membrane disruption, and interference with cellular functions.[5–7] It has been found that there is an improved microbial action when using more than one metallic nanoparticle.[8,9] Depending on the type of nanoparticles used, researchers can create formulations that capitalize on the best characteristics of each particle to achieve optimal antimicrobial effects.[10] Nanoarchitectonics, the concept of purposefully designing and combining nanostructures, is critical for organizing these combinations to provide multiple functionalities for diverse healthcare needs.[11,12] The rationale for selecting Ag, Cu, and Co is their proven ROS-generating activity and the synergistic effect created by doping silica nanoparticles with all three, forming a stable nanoarchitectonic hybrid that enhances

[a]*Department of Chemistry, Faculty of Applied Sciences, University of Sri Jayewardenepura, Gangodawila, Nugegoda, Sri Lanka. E-mail: imalka@sjp.ac.lk; piumikayapa@gmail.com*

[b]*Medical Research Institute, Colombo 8, Sri Lanka. E-mail: drmayuri.geetha@gmail.com*

† Electronic supplementary information (ESI) available. See DOI: https://doi.org/10.1039/d5na00380f

antimicrobial performance and helps overcome resistance mechanisms.[13,14]

However, as the use of nanomaterials expands, there is an increasing need to undertake systematic and integrated evaluations of their safety characteristics. Despite all the positive impacts of nanotechnology, nanoparticles possess many distinct properties that make them potentially hazardous.[15] The toxicity of nanoparticles in the biological system is known as nanotoxicity, which has become an important research interest and a concern.[16] Due to their physical characteristics, nanoparticle exposure has been reported to elicit oxidative stress, inflammation, and genotoxicity due to interference with cellular components. Knowledge of these toxicological consequences is critical to avoid any negative impacts on society in instances where otherwise nanotechnology-tagged applications are laudable.[17,18] Size, form, chemical characteristics, and the method of administering and formulation of nanoparticles also determine their toxicological characteristics. Small nanoparticles (<20 nm) seem to have higher reactivity and bioavailability than large nanoparticles (>20 nm) do. Moreover, the shape of the nanoparticles has an impact on their bioavailability and resulting toxicity in biological systems.[19–22]

The evaluation of nanotoxicity is important for a number of reasons. First, as nanoparticles are being introduced into a range of products, including clothing, food packaging, medical applications, and drugs, there is a need for data on their potential hazard. Potentially useful as NPs may be, unregulated or not well-understood nanoparticles may cause other health effects.[23,24] In addition, safety regulatory authorities such as the FDA and EPA demand full risk evaluation of newly existing nanomaterials. A sound knowledge of nanotoxicity is prudent in offering possible means for regulatory trajectories to be corrected in a bid to portray products that consumers can handle safely.[25] In the biomedical area, nanoparticles have great potential for applications in targeted drug delivery, diagnostics, and antimicrobial coatings; however, these applications mostly remain at their translational stage to clinics until the safety and efficacy of these materials are proven.[26] For this reason, assessing the potential toxicity of nanopharmaceuticals at a nascent stage is of great significance, in an attempt to fine-tune manufacturing processes that will yield substances with high therapeutic activity and low toxicity. In this ever-complicated world, bringing nanotechnology into the fold of healthcare and other disciplines can only be carried out with an understanding of risks and ethical issues.[27]

Because nanotoxicity has many risks, various approaches are being investigated to minimize them. One approach with such an antimicrobial effect is the synergistic addition of different metallic nanoparticles, thus mitigating the toxicity of the nanoparticles while maintaining the efficacy of the antimicrobial effect.[28] However, doping metallic nanoparticles into biocompatible, non-toxic matrices such as silica will still allow the retention of functionality but with improved safety. As can be seen, incorporating metallic nanosystems in medicine means a complete redesign of infection control. New antimicrobial polymer membranes can be made using these nanosystems and be used in personal protection equipment (PPE), wound dressings, and hygiene products. By containing metallic nanoparticles within polymer matrices, these materials can produce consistent protection against microbes, hence decreasing infection susceptibility among sensitive populations.[29] Electrospinning is an ideal method of developing proper matrices that can stabilize these nanosystems for their integration into polymer membranes. This method makes it possible to develop nanofibers with a large surface area and pore size, thereby improving the efficiency of the antimicrobial membranes. By choosing non-irritant and biocompatible polymers, researchers can enhance the safety of the above-mentioned applications, making them suitable for contact with human tissues.[5,7,9]

In order to determine the safety profiles of these developed metallic nanosystems, useful models include *in vivo* models, such as the zebrafish embryo toxicity assay. From this assay, it is possible to compute the LC_{50} values, which are important in fabricating efficient antimicrobial polymer membranes. The LC_{50} value defines the toxic level that will kill 50% of test subjects, therefore that the safety level can be established. The importance of estimating LC_{50} values is not simply confined to toxicity determination; the rates can help design optimum healthcare products that can exhibit powerful impacts and, at the same time, remain virtually harmless to human health. When the toxic levels of these nanosystems are determined, formulation can be made to enhance the antimicrobial properties without causing harm.[30,31]

Furthermore, the hen's egg test-chorioallantoic membrane assay is used as one of the measures in evaluating irritation effects. This test determines the potential of a material to cause irritation to the biological tissues when they come into contact with the developed nanosystems. Moreover, the Franz diffusion cell apparatus is used for diffusion assays so that the skin permeation potential of these nanomaterials can be assessed by researchers. It was also found that knowing the diffusion characteristics is important when evaluating the success of antimicrobial membranes and coatings for usage where the membranes and coatings touch the human skin directly.[32]

The use of alternative models in assessing the safety profiles of metallic nanosystems aligns with the principles of the 3Rs: the three Rs – Replacement, Reduction, and Refinement. These principles maintain the concept of animal usage with emphasis on the least amount of usage as possible while at the same time encoding for valid and reliable results. In this way, using alternatives to *in vivo* models, researchers can collect important data without sacrificing animals.[33,34]

In this study, we present a comprehensive safety profile assessment of an innovative nanofibrous membrane integrated with a metallic nanohybrid system. The antimicrobial efficacy of the metallic nanohybrids was evaluated through the determination of the minimum inhibitory concentration (MIC), minimum bactericidal concentration (MBC) for bacterial species, and minimum fungicidal concentration (MFC) for fungal strains. To assess the toxicity of these nanohybrids, we performed a zebrafish embryo assay to determine the lethal concentration for 50% of the population (LC_{50}). The irritation potential of both the metallic nanohybrids and the nanofibrous

membrane incorporating the nanohybrid system was evaluated using the Hen's Egg Test-Chorioallantoic Membrane (HET-CAM) assay. Additionally, we investigated the skin penetration of metallic nanoparticles from the nanofibers, given that the final product is intended to serve as an antimicrobial functional layer suitable for integration into personal protective equipment (PPE), wound dressings, and personal care products.

2 Materials and methods

2.1 Materials

The reagents, including 3,4-dichloroaniline, sodium chloride, sodium hydroxide, $Na_2HPO_4 \cdot 7H_2O$ (disodium hydrogen phosphate, heptahydrate), KH_2PO_4 (potassium dihydrogen phosphate), KCl (potassium chloride), resazurin, and tricaine methane sulfonate (MS-222), were purchased from Sigma-Aldrich, USA. Silver nitrate ($AgNO_3$), copper chloride ($CuCl_2$), cobalt chloride ($CoCl_2$), tetraethyl orthosilicate (TEOS), glycerol, nitric acid (HNO_3), and liquid ammonia used for the synthesis of metal-doped silica nanohybrids were also obtained from Sigma-Aldrich, USA. HiMedia, India, supplied the analytical-grade chemicals, media, and other materials for microbiology research, including nutrient agar, Mueller–Hinton agar, bacteriological agar, Sabouraud dextrose agar, blood agar, and antibiotic discs. Fertile White Leghorn chicken eggs were obtained from a commercial source. A synthetic, non-animal-based skin model for transdermal diffusion (Strat-M®) was purchased from Merck, Germany.

2.2 Methodology

This study involves the synthesis of monometallic silica nanohybrids, the formulation of multimetallic silica nanohybrids, and the fabrication of electrospun mats that incorporate metallic silica nanohybrids. Additionally, these nanohybrids and nanohybrid-incorporated electrospun mats were characterized in detail based on previously published data from leading authors in this research group.[5,6,10] In addition to our own previous investigations, several other researchers have also demonstrated the significant antimicrobial potential of various metal- and metal oxide-based nanohybrids. For example, Ranathunga *et al.* (2024) reported the preparation and characterization of Fe–ZnO cellulose-based nanofiber mats with self-sterilizing photocatalytic activity for enhanced antibacterial applications under visible light.[7] Peiris *et al.* (2022) evaluated the antibacterial activity of copper and sulfur nanoparticles for controlling bacterial blight caused by *Xanthomonas* sp. in *Anthurium andraeanum* Lind.[8] Similarly, Madhushika *et al.* (2024) highlighted the antimicrobial synergy of polymer-based nanofiber mats reinforced with antioxidants intercalated in layered double hydroxides as potential active packaging materials.[9] Selvaraj *et al.* (2024) further demonstrated the *in vitro* wound healing ability of peptide-loaded cellulose acetate nanofibers with antimicrobial properties.[13] These related studies strongly support the promising antimicrobial applications of nanohybrid systems similar to those explored in our work. Therefore, the present study primarily focuses on evaluating the toxicity and biocompatibility aspects of the synthesized heterometallic silica nanohybrids, complementing the established antimicrobial evidence in the literature.

This article specifically examines the Minimum Inhibitory Concentration (MIC) values of metallic silica nanohybrids, along with their safety profile. The safety assessments include determining the lethal concentration (LC_{50}) for each nanohybrid, evaluating the potential for skin irritation caused by both the metallic silica nanohybrids and the electrospun polymer mats that incorporate these nanohybrids. Additionally, we assess the penetration of metals from the polymer mat into human skin. These safety evaluations were conducted prior to animal testing to adhere to the 3R principles (Replace, Reduce, Refine) and to provide an initial understanding of the nanotoxicity associated with the developed nanohybrids. Fig. 1 shows an illustrative explanation of the methodology.

2.2.1 Synthesis and characterization of metal-doped silica nanohybrids. Cobalt (Co), copper (Cu), and silver (Ag) were selected as dopants for the synthesis of silica-based nanohybrids using a sol–gel method. Silver nitrate ($AgNO_3$), copper chloride ($CuCl_2$), and cobalt chloride ($CoCl_2$) were prepared as 1.5 M salt solutions and mixed (10 mL each) with 10 mL of tetraethyl orthosilicate (TEOS) as the silica precursor, together with 5 mL of glycerol as a templating agent. Acidic hydrolysis was initiated by adding 0.125 M nitric acid dropwise until the pH reached 1.5. The solution was stirred for 3 h with continuous addition of ammonia to adjust the final pH to 8–9. The resulting gel was centrifuged, washed with ethanol, and aged in an ethanol–water system for 48–72 h at room temperature. The dried gels were oven-dried at 100 °C for 1 h and calcined at 500 °C for 5 h to obtain the metal-doped silica nanoparticles. These metal-doped silica nanoparticles (SiNPs) include Ag-doped SiNPs (AgSiNPs), Cu-doped SiNPs (CuSiNPs), and Co-doped SiNPs (CoSiNPs). To prepare trimetallic nanohybrids, monometallic nanohybrids were combined in equal ratios and dispersed in ultra-pure water under ultrasonication.[5,6,10]

The synthesized nanohybrids were characterized *via* X-ray diffraction (XRD) using a Rigaku SmartLab diffractometer (3 kW sealed X-ray tube, CBO optics, D/teX Ultra 250 silicon strip detector) within a scanning range of 10°–85° (2θ). The surface morphology and particle structure were examined by scanning electron microscopy (SEM) with a ZEISS microscope (secondary electron mode, 10 kV accelerating voltage) and by transmission electron microscopy (TEM) using a JEOL JEM-2100 (operating at 20 kV). Elemental composition and metal distribution were confirmed by energy-dispersive X-ray spectroscopy (EDX) performed in parallel with SEM imaging.[5,6,10]

2.2.2 Assessing the Minimum Inhibitory Concentration (MIC), Minimum Bactericidal Concentration (MBC), and Minimum Fungicidal Concentration (MFC) of the metallic silica nanohybrids. The Minimum Inhibitory Concentration (MIC) of monometallic and trimetallic nanohybrids was determined by the microdilution method, using 96-well microtiter plates. The monometallic nanohybrids, including Ag-doped silica nanoparticles, Cu-doped silica nanoparticles, and Co-doped silica nanoparticles, and the trimetallic silica nanohybrids, including Ag, Cu, CoSiNPs, were tested. Commercially available standard antibiotics were used as positive controls;

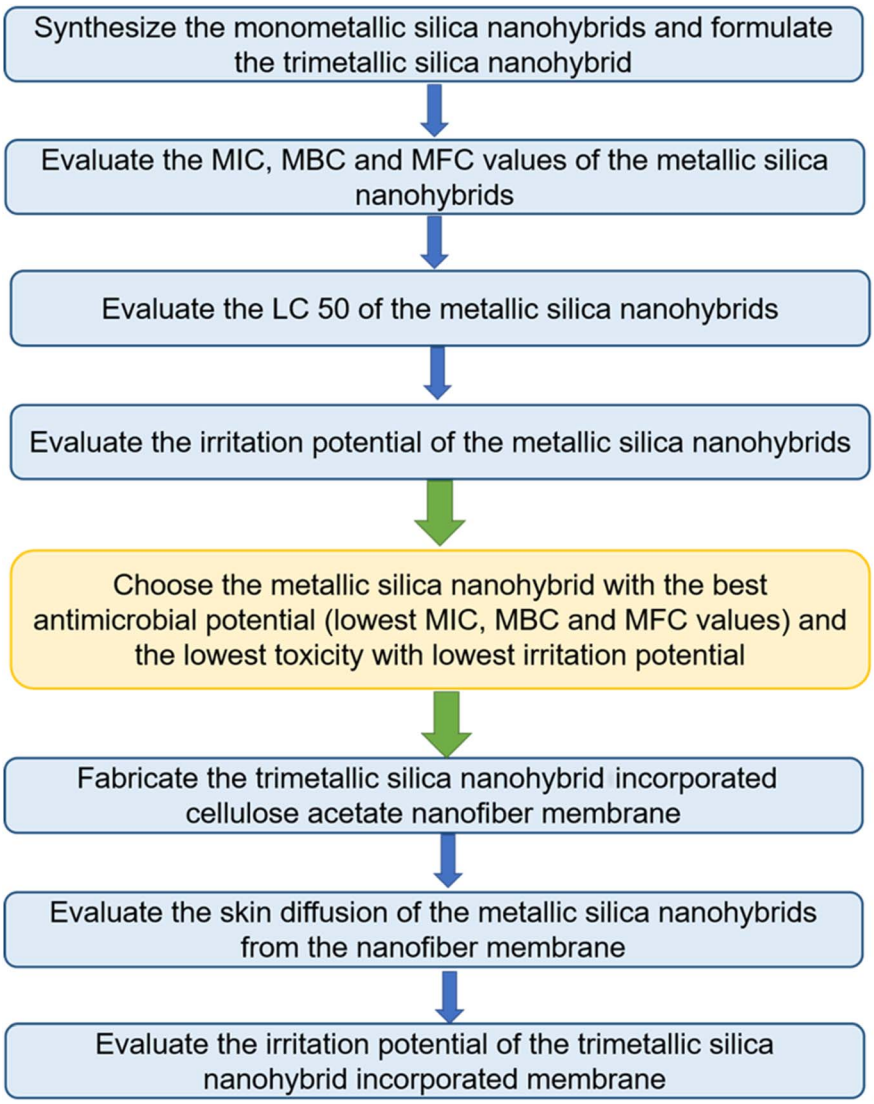

Fig. 1 An illustrative description of the methodology used in the study.

erythromycin was used for Gram-positive bacteria, gentamycin was used for Gram-negative bacteria, and fluconazole was used for fungi. A series of two-fold dilutions of metallic nanohybrids in a concentration range (100 mg mL^{-1} to 0.047 μg mL^{-1}) with adjusted bacterial concentration (10^8 CFU mL^{-1}, 0.5 McFarland's standard) was used to determine the MIC in MHA broth. Six strains of bacteria, including Gram-positive bacteria: *Staphylococcus aureus* (ATCC 25923), *Streptococcus pneumoniae* (ATCC 49619), and methicillin-resistant *Staphylococcus aureus* (MRSA), and Gram-negative bacteria: *Escherichia coli* (ATCC 25922), *Klebsiella pneumoniae* (ATCC BAA 1706), and *Pseudomonas aeruginosa* (ATCC 27853), and four strains of fungi, including *Candida albicans* (ATCC 10231) and quality control samples of *Trichophyton rubrum*, *Microsporum gypseum*, and *Aspergillus niger*, were used as test microorganisms. The negative control contained only inoculated broth.

The plates were incubated for 24 h at 37 °C. The MIC endpoint is the lowest concentration of metallic nanohybrids where no visible growth is observed in the wells. The visual turbidity of the wells was noted, both before and after incubation, to confirm the MIC value. Then, a volume of 20 μL of resazurin dye solution (0.01% (w/v)) was added to each well and incubated all 96 well plates for another 2 hours at 37 °C. The resazurin assay, also known as the Alamar Blue assay, detects viable cells after growth in a culture medium. The principle of this test is based on the visual detection of the reduction of the resazurin reagent, a viability colorant, as observed by its color change (blue to purple or pink). Therefore, the MIC values were determined by considering the colour change of the resazurin dye solution; the point at which the colour change of the dye began from blue to pink was noted as the MIC point for each microorganism.

To evaluate the MBC value for each nanohybrid against the tested bacteria, the broths were subcultured on freshly prepared agar plates. Five broths were subcultured for each nanohybrid: the MIC point, three consecutive concentrations above the MIC point, and one concentration below the MIC point. Then all the sets of plates were incubated for 24 hours at 37 °C. The colony count on each plate was noted, and the plate with the zero-

colony count was evaluated as the MBC point. All the procedures were triplicated and conducted according to the CLSI guidelines.[5,10]

2.2.3 Evaluating the acute toxicity of the metallic nanohybrids by LC_{50} values using the zebrafish embryo toxicity assay (ZFET). Acute toxicity is usually determined with short-term exposure of zebrafish eggs to a series of concentrations of chemicals. Initially, female and male zebrafish (*Danio rerio*) were allowed to mate, and fertilized eggs were collected within 30 minutes of fertilization. Then the live eggs were placed in sterile 24-well plates. Subsequently, the embryos were treated in different concentrations of the synthesized nanohybrids. Indications of death of an embryo include coagulation of the embryo, lack of somite formation (a somite is an early-stage division of a body part of an embryo that eventually goes on to form vertebrate, skeletal muscle, cartilage, tendons, and skin of the back), non-detachment of the tail, and/or lack of heartbeat. All are easily detectable using light microscopy.

In this study to assess the nanotoxicity of metallic silica nanohybrids, including AgSiNPs, CuSiNPs, CoSiNPs, and trimetallic SiNPs, seven concentrations (10.000–0.156 mg L^{-1}) of each were used, and the observations were recorded. All the test procedures were performed according to the OECD guidelines 236 (OECD, 2013) with slight modifications.[35] Twenty eggs were used for each test concentration ($n = 20$) with three replicates, and each replicate had an internal plate control with ultra-pure water. 2,3-Dichloroaniline (4 mg L^{-1}) was used as the positive control. An internal control containing ultra-pure water and one whole plate maintained with ultra-pure water served as the negative control. Four apical points described in the introduction were recorded under the optical microscope at different time points throughout the experimental period (24–96 h).

To quantify the observed toxicity, a scoring system was used based on the toxicity level of a particular material, and instead of endpoint assessment, the severity of toxicity was graded by introducing a grading system. Each endpoint was assigned a score based on its severity: one point was awarded if there were deceased embryos, malformations, or developmental delays; each dead embryo was given one point, each malformation was given one point, and each developmental delay seen was also given one point. The statistical comparison was performed using the Wilcoxon signed-rank test. Afterward, the individual apical points for each concentration level were obtained by summing the scores in each of the assessed endpoints and presented as a percentage of the overall toxicity measure in that concentration. The regression model and probit analysis were used to calculate the LC_{50} values. Then the LC_{50} values were compared to determine the toxicity of metallic silica nanohybrids. Finally, a two-sample *t*-test was performed at a significance level of $p = 0.05$ to statistically confirm the differences between LC_{50} values of the trimetallic silica nanohybrid compared to the monometallic silica nanohybrid. All the plates containing experimental embryos were placed in a fish room under controlled light and temperature conditions (*i.e.*, temperature 26 °C ± 1 °C with a 14 h/10 h light/dark cycle) throughout the experiment.[35]

2.2.4 Calculating the therapeutic index of each nanohybrid against tested microbes. The therapeutic index (TI) was calculated to evaluate the relative safety and antimicrobial effectiveness of the synthesized nanohybrids. The TI was determined using the following equation:

$$\text{Therapeutic index(TI)} = \frac{EC_{50}}{LC_{50}}$$

In this study, the minimum inhibitory concentration (MIC) for each microbe was used as the ED_{50}, representing the minimum effective dose of the nanohybrids. The LC_{50} values were obtained from the zebrafish embryo toxicity test. Therapeutic indices were calculated for all tested microbes by dividing the corresponding LC_{50} (mg L^{-1}) by the MIC (mg mL^{-1}) for each nanohybrid.[36]

2.2.5 Assessing the skin irritation potential of metallic silica nanohybrids and the electrospun polymer mat incorporated with trimetallic silica nanohybrids. In this study, we used the HET-CAM assay to evaluate the irritation potential of several types of silica-based nanohybrids, originating from the silver-doped silica nanoparticles (Ag–SiNPs), copper-doped silica nanoparticles (Cu–SiNPs), cobalt-doped silica nanoparticles (Co–SiNPs), and trimetallic silica nanoparticles. The decision to employ HET-CAM for the evaluation of skin irritation was due to the need for efficient methods of localization of materials used in the dermatological market, especially with regard to nanomaterials and their effects on the skin.

While unconventional, using HET-CAM for assessing skin irritation is scientifically justified. Numerous high-impact publications have reported the successful adaptation of the HET-CAM assay for evaluating vaginal irritation, demonstrating the method's versatility beyond ocular assessments.[37] The chorioallantoic membrane provides a biological environment that reflects the complexities of human tissue responses, including vascularization and sensitivity to irritants. Furthermore, quantifying responses such as hemorrhage, lysis, and coagulation adds a layer of sensitivity to irritation detection that is particularly relevant in evaluating skin-compatible materials.[38]

Fertile White Leghorn chicken eggs were purchased from a local commercial supplier (Nishadani Poultry Breeder Farm, Radawana, Gampaha, Sri Lanka). Chosen eggs were fresh and in the weight range of 50–60 grams. Prior to using the eggs, the embryos were checked for their viability by a process known as candling, whereby unviable, defective, or eggs that were too twisted or cracked were discarded. The essential materials used in the experiment included a candling lamp, ultrapure water, surgical scissors, an incubator, and micropipettes with disposable tips suitable for the volume ranges recommended in the study. Furthermore, a mortar and pestle, other grinding facilities, a stop clock, and common biological laboratory facilities such as microcentrifuge tubes, tapered forceps, and volumetric flasks were also used.

Stock solutions were made volumetrically. A 0.9% (w/v) sodium chloride solution in ultra-pure water was used as the negative control, and a 0.1 N sodium hydroxide solution in ultra-pure water was used as the positive control. The dispersions of synthesized silica nanohybrids, including Ag–SiNPs, Cu–SiNPs, Co–SiNPs, and trimetallic SiNPs, were prepared by

dispersing them in ultrapure water. Each test solution was prepared to contain a final concentration of 100 mg L^{-1}.

In each experiment, a negative control solution of 0.9% (w/v) NaCl was included to determine the level of background skin reaction and to eliminate the possibility of the assay system causing an undesirable irritant response. A positive control using 0.1 N NaOH, a solution known to inflict eye irritation. was also used to ensure that the unwanted response was being induced by the assay.[38]

Three eggs per group were utilized in this set of experiments: negative and positive controls, as well as the test samples. Healthy, clean, and fertile White Leghorn chicken eggs of approximately 50–60 g were used, and any unsuitable eggs were dismissed after candling. Rejects were also eggs with abnormal shapes or severely damaged shells. On day eight, the eggs were candled in order to eliminate weak eggs, and the good ones were incubated for one more day. On the ninth day, all eggs laid were transferred out of the incubator and candled again. A specific area on every air cell of eggs was labeled, and the egg was then placed in a vise with a proper orientation such that no inner membrane would be pried off when the air cell cap was obtained by cutting through it using surgical scissors. The inner membrane was moisturized with 0.9% NaCl solution using a disposable glass pipette, and the egg was incubated for no more than 30 minutes after its application. After incubation, 0.9% NaCl solution was gently pipetted off, and the inner membrane was then picked up at the corner using forceps.[38]

A volume of 0.3 mL of nanohybrid dispersions (concentration = 100 mg L^{-1}; 100 mg of the nanohybrids in 1 L of ultrapure water) was pipetted on the CAM. An identical volume of 0.3 mL was pipetted over the CAM for both the negative and positive controls. Interactions of reactions on the CAM were detected for 300 seconds, while the appearance of the endpoints, such as hemorrhage, vascular lysis, and coagulation, was in seconds. The time for hemorrhage, the degree of arterial and venous filling, the vascular lysis, and the coagulation time were measured. Hemorrhage was defined by the onset of bleeding from vessels, whereas vascular lysis was defined by the onset of blood vessel disintegration, and coagulation was defined by the onset of protein conformation change (intra- and extra-vascular).

The possible HET-CAM endpoint scores obtained were inspected in total using the ICCVAM IS (A) analysis type. This entailed adding the time-dependent scores for lysis, hemorrhage, and coagulation. The scoring for irritation testing was as follows:

	Score		
Effect	0.5 min	2 min	5 min
Lysis	5	3	1
Hemorrhage	7	5	3
Coagulation	9	7	5

These include the total of scores for lysis, hemorrhage, and coagulation at the time intervals specified above. The total possible mark was twenty-one for this knowledge test. The interpretation of the total irritation score was as follows:[38]

0–9: non-irritating, 10–21: irritating.

Finally, a two-sample *t*-test was performed at a significance level of $p = 0.05$ to statistically confirm the differences between irritation scores of the trimetallic silica nanohybrid compared to monometallic silica nanohybrid.

2.2.6 Evaluating the skin penetration of the fabricated trimetallic SiNP-incorporated nanofiber membrane. The skin permeation of the synthesized nanohybrids was determined using a Franz diffusion cell according to the OECD guideline 428.[39,40] An electrospun cellulose acetate nanofibrous membrane was prepared to anchor the synthesized nanohybrids in the application of antimicrobial activity. Among the synthesized nanohybrids, Trimetallic SiNPs were chosen because they exhibited higher antimicrobial activity with the lowest toxicity, as analyzed through MIC, MBC, LC_{50}, and skin irritation scores superior to the monometallic metal nanoparticular forms such as Ag, Cu, and Co.

For practical use, these nanohybrids were incorporated and entrapped within a polymer membrane synthesized for this purpose. After the fabrication of the membrane, the skin penetration of the individual metals – Ag, Cu, and Co – was determined by ICP-MS analysis to evaluate the penetration depths of the metals through the membrane. This procedure enabled one to evaluate the efficacy of penetration of every metal as well as its possibility for direct antimicrobial use. A synthetic membrane, chosen as the model membrane for the skin penetration study, was the Merck Strat-M membrane with a diameter of $d = 2.5$ cm.

Importantly, the Franz diffusion cell system comprises basic components of a donor chamber, a receptor chamber, and the skin membrane. The skin membrane used for the study was mounted between the donor chamber and the receptor chamber with the epidermal side towards the donor chamber. The donor chamber was loaded with the test substances, consisting of synthesized nanohybrid formulations dissolved in the appropriate solvents to obtain a controlled concentration. Under physiological conditions, the receptor chamber was filled with receptor medium, which was commonly used phosphate-buffered saline (PBS). The temperature in both chambers was regulated using a water jacket to a more accurate bodily skin temperature of 32 °C.[39,40]

A fixed concentration of the test material incorporating the nanohybrids was applied onto the donor chamber so as to provide an even distribution on the skin. The donor chamber was specially sealed in order to minimize evaporation and the access of contaminants into the sample. Since the rate of permeation through the skin membrane was not known ahead of time, samples were taken from the receptor chamber at time intervals of 12 and 24 hours to determine how much of the test substance had penetrated the skin. The receptor fluid was replaced with fresh PBS to maintain the volume of the solution since diffusion takes place based on a concentration gradient. The withdrawn samples were kept at −20 °C until the time of assay.

In every experiment, a negative control formulation that lacked the nanohybrids but had all other components was used to eliminate any contamination or interference possibilities. A

positive control, phenol, was also used to validate the functionality of the diffusion system.[39]

3 Results and discussion

A detailed safety analysis of innovative nanofibrous membranes combined with metallic nanohybrids (Fig. 2) exists in this study. The antimicrobial effects of metallic nanohybrids were studied through MIC and MBC assessment for bacteria and MFC evaluation for fungal strains. The zebrafish embryo toxicity assay was employed to determine the lethal concentration that kills 50% of the population, known as LC_{50}. An evaluation of irritation potential applied to the metallic nanohybrids alongside the nanofibrous membrane, with the nanohybrid system utilized the Hen's Egg Test-Chorioallantoic Membrane (HET-CAM) assay. Moreover, we tested the ability of metallic nanoparticles to penetrate human skin through these nanofibers because the final application will use the antimicrobial functional layer as an integration component in personal protective equipment (PPE), wound dressings, and personal care products.

3.1 Characterization of metallic silica nanohybrids

To verify the successful synthesis of metal-doped silica nanoparticles, X-ray diffraction (XRD) analysis was first conducted (Fig. 3a). The XRD patterns confirmed the presence of crystalline phases corresponding to each doped metal, along with the characteristic amorphous nature of the silica matrix. A broad, low-intensity peak between $2\theta = 25$–$30°$ indicated the amorphous SiO_2 structure across all samples. For AgSiNPs, distinct diffraction peaks at 2θ values from 15° to 85°, indexed to the (111), (200), (220), (311), and (222) planes, confirmed the face-centered cubic (fcc) crystalline structure of silver oxide (AgO), matching JCPDS no. 04-0783.

Similarly, the CuSiNPs displayed well-defined peaks corresponding to copper oxide (CuO), with planes indexed to (110), (002), (−111), (111), (200), (−112), and others, aligned with JCPDS no. 05-0661. The CoSiNPs exhibited multiple peaks assigned to Co_3O_4 crystalline phases, including (111), (220), (311), and higher-order planes, consistent with JCPDS no. 42-1467. The trimetallic silica nanohybrid showed diffraction peaks for AgO, CuO, and Co_3O_4 simultaneously, confirming the coexistence of all three metal oxides within the silica network. Due to the complexity of the hybrid structure, some individual peaks observed in monometallic samples may overlap or diminish in intensity within the trimetallic system.[5,6]

Subsequently, the nanohybrids were examined for their morphology using SEM and TEM imaging (Fig. 3b and c). The SEM and TEM images confirmed the successful doping of metals into the silica framework, with particles retaining an overall spherical shape. SEM images (Fig. 3b(i)–(iv)) illustrate the surface morphology of the Ag-, Cu-, Co-doped, and trimetallic SiNPs, respectively, showing uniform dispersion and nanoscale features. The TEM images (Fig. 3c(i)–(iv)) further confirmed the porous structure and clear spherical form of the particles, with darker regions indicating the distribution of metal dopants within the silica matrix. The observed lattice fringes in high-resolution TEM images correspond well with the *d*-spacing values derived from XRD analysis, supporting the crystalline nature of the embedded metal oxides.[5,6]

Elemental distribution was further analyzed by energy-dispersive X-ray (EDX) mapping (Fig. 3d). The EDX elemental maps demonstrated the homogeneous presence and distribution of oxygen, silicon, and the respective doped metals (Ag, Cu, and Co) throughout the nanohybrid structures. This uniform distribution confirmed the effective doping and integration of metal species within the silica framework, supporting the intended nanoarchitectonic design for enhanced antimicrobial activity.[5,6]

3.2 Evaluation of the MIC, MBC, and MFC of the metallic silica nanohybrids

The antimicrobial properties of this metallic nanohybrid system were examined against multiple bacterial strains, together with different fungal strains, which included Gram-positive and Gram-negative bacteria and fungi. This study evaluated the bacterial strains of *Staphylococcus aureus* (ATCC 25923), *Streptococcus pneumoniae* (ATCC 49619), methicillin-resistant *Staphylococcus aureus* (MRSA), *Escherichia coli* (ATCC 25922),

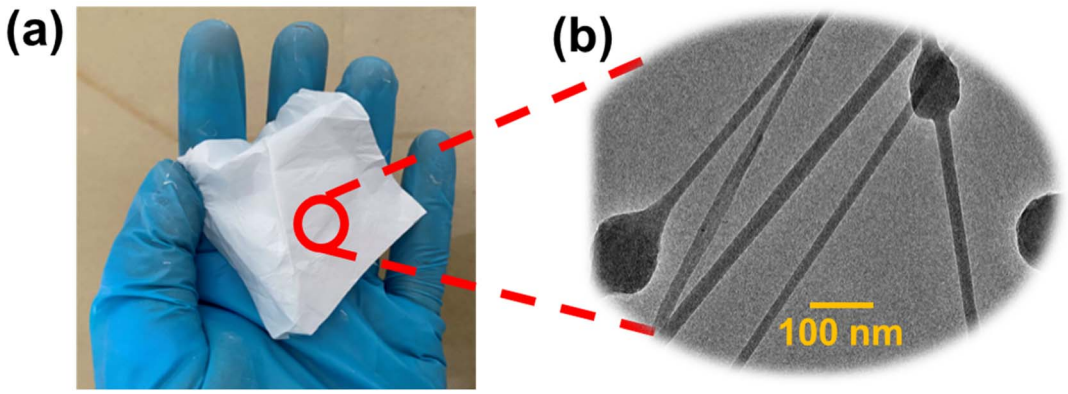

Fig. 2 (a) A digital photograph and (b) TEM image of the fabricated nanofibrous membrane, which is incorporated with trimetallic silica nanohybrids (scale = 100 nm).

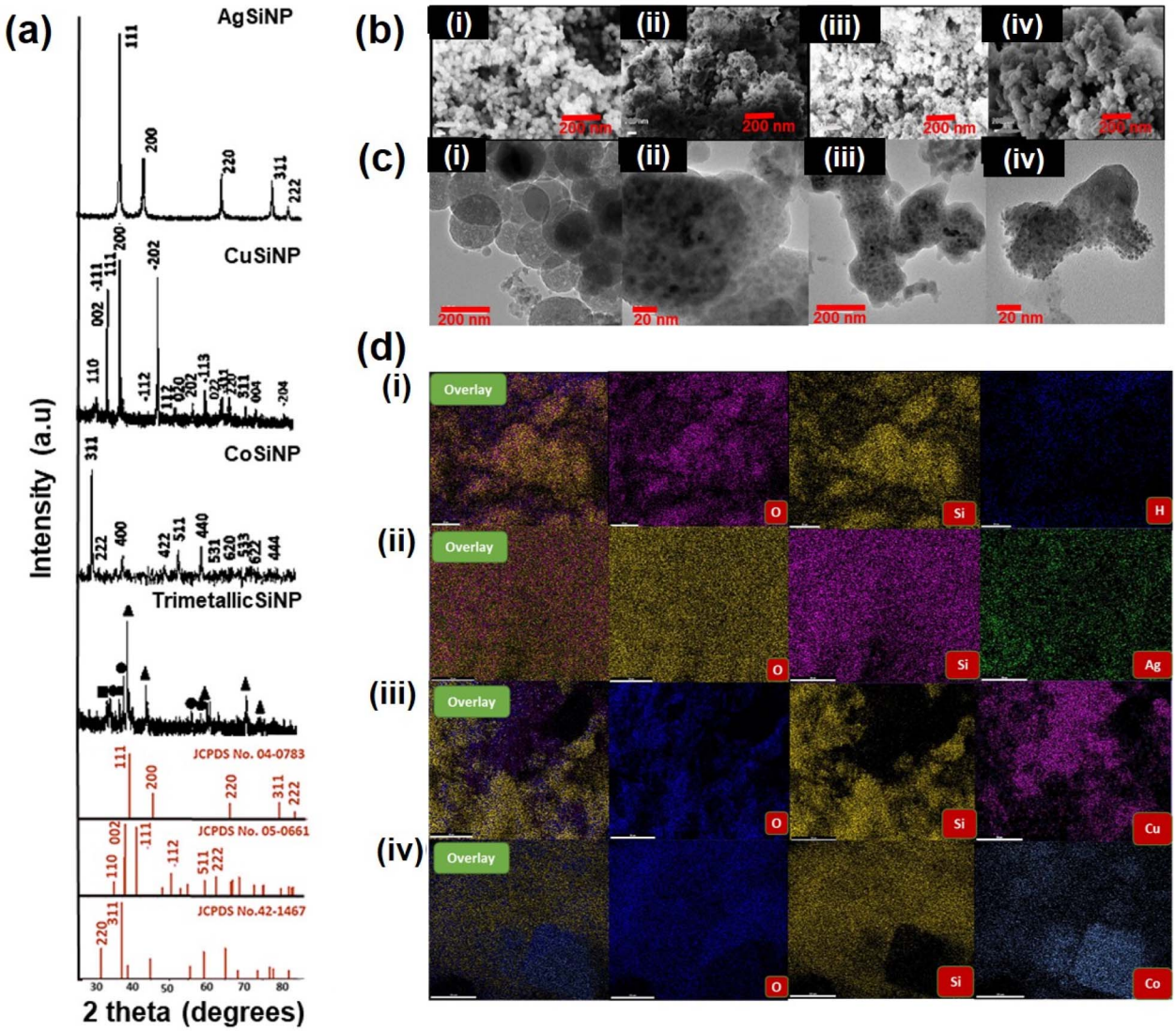

Fig. 3 Characterization of synthesized metal-doped silica nanohybrids; (a) X-ray diffraction (XRD) patterns of AgSiNPs, CuSiNPs, CoSiNPs, and trimetallic silica nanohybrids; ▲ AgSiNP, ● CuSiNP and ■ CoSiNP; (b) SEM and (c) TEM images showing the surface morphology and internal structure of (i) SiNPs, (ii) AgSiNPs, (iii) CuSiNPs, and (iv) CoSiNPs; (d) energy-dispersive X-ray spectroscopy (EDX) elemental mapping for (i) SiNPs, (ii) AgSiNPs, (iii) CuSiNPs, and (iv) CoSiNPs.

Klebsiella pneumoniae (ATCC BAA 1706), and *Pseudomonas aeruginosa* (ATCC 27853). The investigation used *Candida albicans* (ATCC 10231) together with *Trichophyton rubrum*, *Microsporum gypseum*, and *Aspergillus niger* as the tested fungal strains.[5,7,10]

The research determined Minimum Inhibitory Concentration (MIC), Minimum Bactericidal Concentration (MBC), and Minimum Fungicidal Concentration (MFC) values for every bacterial strain under study. The MIC values show the minimum preventive concentration of nanohybrids against microbial development, while MBC and MFC values indicate the required amount to destroy 99.9% of the microorganisms. All tested bacterial and fungal strains yielded their results for MIC through these assays, as shown in Table 1. The established values represent a complete picture of how potent the nanohybrid system is against antimicrobial agents.

Then, the MBC values of the nanohybrids against bacterial strains and the MFC values of the nanohybrids against fungal strains were evaluated. Table 2 shows the respective values for MBC and MFC. The numbers recorded during MBC tests indicated similar antibacterial properties of the nanohybrid as the MIC tests showed for bacterial strains. The nanohybrid system exhibits properties to kill microbes at near-inhibitory concentration levels alongside its capability to restrict microbial growth. The nanohybrid showed robust antifungal effects against *C. albicans* and *A. niger* among several fungal strains because its minimum fungal concentration values remained low.

The nanohybrid system needed higher concentrations of testing solution than the standard antibiotic for microbial growth inhibition, according to MIC values. Tests conducted on

Table 1 The evaluated MIC values for each nanohybrid[a]

Type of the nanofiber mat/Standard antibiotic	MIC values (μg mL^{-1})									
	S. aureus	*S. pneumoniae*	MRSA	*E.coli*	*K. pneumoniae*	*P. aeruginosa*	*C. albicans*	*T. rubrum*	*M. gypseum*	*A. niger*
Positive control	12.50 ± 0.00	9.72 ± 0.00	12.50 ± 0.00	12.50 ± 0.00	12.50 ± 0.00	12.50 ± 0.00	24.50 ± 0.00	24.50 ± 0.00	24.50 ± 0.00	24.50 ± 0.00
Negative control	0.00 ± 0.00	0.00 ± 0.00	0.00 ± 0.00	0.00 ± 0.00	0.00 ± 0.00	0.00 ± 0.00	0.00 ± 0.00	0.00 ± 0.00	0.00 ± 0.00	0.00 ± 0.00
1	97.00 ± 0.00	49.00 ± 0.00	97.00 ± 0.00	97.00 ± 0.00	197.00 ± 0.00	197.00 ± 0.00	97.00 ± 0.00	49.00 ± 0.00	97.00 ± 0.00	97.00 ± 0.00
2	197.00 ± 0.00	197.00 ± 0.00	197.00 ± 0.00	197.00 ± 0.00	197.00 ± 0.00	197.00 ± 0.00	197.00 ± 0.00	197.00 ± 0.00	197.00 ± 0.00	197.00 ± 0.00
3	780.00 ± 0.00	780.00 ± 0.00	780.00 ± 0.00	1560.00 ± 0.00	1560.00 ± 0.00	1560.00 ± 0.00	780.00 ± 0.00	780.00 ± 0.00	780.00 ± 0.00	1560.00 ± 0.00
4	24.50 ± 0.00	24.50 ± 0.00	24.50 ± 0.00	24.50 ± 0.00	49.00 ± 0.00	49.00 ± 0.00	24.50 ± 0.00	24.50 ± 0.00	24.50 ± 0.00	24.50 ± 0.00

[a] 1 = AgSiNP, 2 = CuSiNP, 3 = CoSiNP, and 4 = trimetallic silica nanohybrid.

Table 2 The evaluated MBC and MFC values for each nanohybrid[a]

Type of the nanofiber mat/standard antibiotic	MBC/MFC values (μg mL^{-1})									
	Bacteria						Fungi			
	S. aureus	*S. pneumoniae*	MRSA	*E. coli*	*K. pneumoniae*	*P. aeruginosa*	*C. albicans*	*T. rubrum*	*M. gypseum*	*A. niger*
Positive control	12.50 ± 0.00	9.72 ± 0.00	12.50 ± 0.00	12.50 ± 0.00	12.50 ± 0.00	12.50 ± 0.00	24.50 ± 0.00	24.50 ± 0.00	24.50 ± 0.00	24.50 ± 0.00
Negative control	0.00 ± 0.00	0.00 ± 0.00	0.00 ± 0.00	0.00 ± 0.00	0.00 ± 0.00	0.00 ± 0.00	0.00 ± 0.00	0.00 ± 0.00	0.00 ± 0.00	0.00 ± 0.00
1	390.00 ± 0.00	197.00 ± 0.00	390.00 ± 0.00	390.00 ± 0.00	390.00 ± 0.00	390.00 ± 0.00	97.00 ± 0.00	49.00 ± 0.00	97.00 ± 0.00	97.00 ± 0.00
2	780.00 ± 0.00	780.00 ± 0.00	780.00 ± 0.00	780.00 ± 0.00	780.00 ± 0.00	780.00 ± 0.00	197.00 ± 0.00	197.00 ± 0.00	197.00 ± 0.00	197.00 ± 0.00
3	1560.00 ± 0.00	3125.00 ± 0.00	1560.00 ± 0.00	1560.00 ± 0.00	1560 ± 0.00	3125.00 ± 0.00	780.00 ± 0.00	780.00 ± 0.00	780.00 ± 0.00	1560.00 ± 0.00
4	49 0.00 ± 0.00	97.00 ± 0.00	97.00 ± 0.00	97.00 ± 0.00	197.00 ± 0.00	197.00 ± 0.00	24.50 ± 0.00	24.50 ± 0.00	24.50 ± 0.00	24.50 ± 0.00

[a] 1 = AgSiNP, 2 = CuSiNP, 3 = CoSiNP, and 4 = trimetallic silica nanohybrid.

four nanohybrid groups identified dissimilar results between each other. Ag SiNP (1), along with Cu SiNP (2), displayed MIC values that fell into a similar range between 97 μg mL^{-1} and 197 μg mL^{-1} for Gram-positive bacteria testing. However, Co-SiNP (3) together with trimetallic silica nanohybrid (4) exhibited lower MIC values when they were both assessed against *S. aureus* and *S. pneumoniae* bacteria, which suggests that the trimetallic combination provides enhanced antimicrobial effectiveness. The combined silver, copper, and cobalt elements in trimetallic silica nanohybrid (4) exhibited synergistic performance, which provided enhanced antimicrobial activity against Gram-positive bacterial and fungal strains *C. albicans* and *A. niger*. The combined metals in the trimetallic nanohybrid operate through synergistic effects that produce an antimicrobial effect that exceeds that of each component alone. The MIC outcomes for Gram-negative bacteria against the nanohybrids extended from 197 μg mL^{-1} to 1560 μg mL^{-1}. Gram-negative bacteria display an outer membrane barrier that restricts antimicrobial penetration into the bacterial cell, as one would expect. The antimicrobial performance of trimetallic silica nanohybrid (4) surpassed metal-doped SiNPs in tests against *P. aeruginosa* and *K. pneumoniae* because its three-metal composition reinforced antibacterial effects toward these hard-to-kill pathogens.[41–43]

A similar pattern emerged from the evaluation of MBC and MFC testing methods, which determine the microbial population reduction to 99.9%. Bacteriostatic effects occur at lower concentrations as the MBC values exceed MIC values for bacteria when using the nanohybrid system. Fungal MFC values exhibited wider ranges, starting from 97 μg mL^{-1} and reaching up to 3125 μg mL^{-1}. A synergistic antifungal effect emerges from the trimetallic composition in nanohybrid (4), which results in superior fungicidal activity against the fungi *T. rubrum* and *M. gypseum* when compared to other nanohybrids because of its lower MFC values.[44,45]

The antimicrobial effects produced from the trimetallic silica nanohybrid (4) stem from the joint action between silver (Ag), copper (Cu), and cobalt (Co) ions. The combination of silver and copper metals with cobalt generates antibacterial effects that enhance material antimicrobial properties due to their established antimicrobial potential. The antimicrobial properties of silica matrix-based nanohybrids improve because the chemical interactions between metals boost their total antimicrobial effectiveness against microbes. Consequently, trimetallic nanohybrids function as more effective antimicrobial agents than metal-doped SiNPs.[41,44]

The antimicrobial efficiency of trimetallic silica nanohybrid (4) outperformed individual particles—AgSiNP (1), CuSiNP (2), and CoSiNP (3)—due to the synergistic collaboration of the three metal ions. The antimicrobial performance of the mixture improved its ability to destroy Gram-positive bacteria and fungi in addition to maintaining strong efficacy against Gram-negative bacteria. The antimicrobial features of trimetallic nanohybrid systems indicate strong potential for medical and hygiene-related products and personal protective equipment, as well as wound care applications.[5,7,10]

3.3 Evaluation of the acute toxicity of the metallic nanohybrids by LC_{50} values using the zebrafish embryo toxicity assay (ZFET)

The Zebrafish Embryo Test (ZFET) measured nanohybrid toxicity using the lethal concentration for 50% of the population (LC_{50}) evaluation based on the OECD guideline 236 with adapted procedures. Early developmental material screening depends on this assay as a dependable technique to detect potentially hazardous effects. The study evaluated AgSiNPs, CuSiNPs, CoSiNPs, and trimetallic silica nanohybrids for their toxicity levels through LC_{50} value assessments. The positive control utilized 2,3-dichloroaniline, with Milli-Q water used as the negative control. The zebrafish embryonic development revealed four significant signs indicating developmental toxicity: embryo coagulation, somite failure, tail non-detachment, and no heart activity. Table 3 shows the calculated LC_{50} values for each nanohybrid.

The results obtained through Zebrafish Embryo Test (ZFET) measurements show the toxicity strength of various nanohybrid materials as measured by LC_{50} values. These measurements indicate the lethal concentration that results in the mortality of 50% of zebrafish embryos, and stronger toxicity corresponds to lower LC_{50} values. AgSiNPs proved to be the most toxic nanohybrid since the LC_{50} measurement reached 2.05 mg L^{-1}. Ag-doped SiNPs exhibit higher toxic properties because they need lower exposure concentrations to achieve lethal effects based on the established antimicrobial and cytotoxic properties of silver nanoparticles. The toxicity level of silver nanoparticles remains elevated because these particles naturally attach to biological elements, thus leading to this study outcome.

Analysis showed that CuSiNPs were less toxic than AgSiNPs because they presented a LC_{50} value of 5.53 mg L^{-1}. The antimicrobial effects of copper nanoparticles occur simultaneously with lower toxicity toward living organisms, as shown by the higher LC_{50} value measured compared to silver nanoparticles. The antimicrobial function of copper-doped nanohybrids remains effective because they demonstrate reduced toxic properties. The Co-doped SiNPs exhibited minimum toxicity toward microbes because their LC_{50} value reached 9.99 mg L^{-1} and exceeded that of other single-metal doped SiNPs. Cobalt nanoparticles demonstrate reduced toxicity as compared to silver and copper nanoparticles, therefore producing the reported higher LC_{50} value. The high LC_{50} value indicates that Co-doped SiNPs represent a safer option for medical applications requiring minimal toxicity, including wound care and medical devices.

Table 3 The calculated LC_{50} values for each nanohybrid

Nanohybrid	LC_{50} (mg L^{-1})
AgSiNP	2.05
CuSiNP	5.53
CoSiNP	9.99
Trimetallic silica nanohybrid	6.35

The antimicrobial potential of trimetallic silica nanohybrid containing silver, copper, and cobalt-doped SiNPs achieved a toxicity level of 6.35 mg L^{-1} during the experiment. The measurements demonstrate that the trimetallic nanohybrids exhibited toxicity between the Co-doped SiNPs and both Ag-doped SiNPs and Cu-doped SiNPs. The three-metal combination in trimetallic nanohybrids creates balanced antimicrobial effects and toxicity that provides regulated toxic effect release compared to single-metal SiNP nanohybrids. The trimetallic nanohybrid demonstrates an optimal antimicrobial effect, which positions it as an excellent choice for applications that need careful coordination of antimicrobial performance and safety levels.

All performed LC_{50} analyses demonstrated the toxic properties of nanohybrids, which depend on their administered doses. AgSiNPs exhibit strong antimicrobial capabilities but are also highly toxic to living cells, so they might not be suited for several biomedical functions. The Co-doped SiNP emerges as the safer option among these nanohybrids; however, the trimetallic silica nanohybrid provides a medium range of toxicity, which enhances its potential applicability. The analysis reveals why nanohybrid formulations must reach proper antimicrobial effectiveness and safety levels for biomedical applications that involve wound dressings and personal protective equipment. Fig. 4 shows the graph of LC_{50} values and the statistical analysis of the LC_{50} values of each nanohybrid.

The two-sample *t*-test was executed to perform, statistical analysis for evaluating toxicological variations between monometallic SiNPs and trimetallic SiNPs at a significance threshold of 0.05. The research showed a substantial variation between the half lethal concentration (LC_{50}) points of the trimetallic silica nanohybrid in comparison to single metal-doped SiNPs. Statistical testing showed that trimetallic SiNPs exhibited more toxicity than Co-doped SiNPs using a significance value of (*) and more than Cu-doped SiNPs (**) while surpassing Ag-doped SiNPs (***). The trimetallic content in SiNPs produces toxicity results dissimilar to those of the monometal-doped SiNPs. The results showed that trimetallic SiNPs had dissimilar LC_{50} values compared to the Co-doped SiNPs, Cu-doped SiNPs and Ag-doped SiNPs because the multiple metals present in the trimetallic nanohybrid fundamentally reshape its toxic characteristics. Research data support that the toxicity characteristics of the trimetallic system lie between its individual metal components, depending on the specific compositional blend. Statistical results indicate that the trimetallic SiNP formulation demonstrates toxicity effects unlike the single-metal SiNPs, such as CoSiNPs. The data show that the judgment needs to account for multiple metal interactions when developing nanomaterials intended for biomedical functions because metal combinations produce substantial modifications in material safety and antimicrobial effects. Moreover, statistical comparisons confirm that every LC_{50} value differs from its counterparts, which demonstrates that each nanohybrid formulation presents different toxicity characteristics because no two nanohybrids have matching toxicity thresholds; thus, nanomaterial selection demands consideration of specific application needs alongside safety concerns.

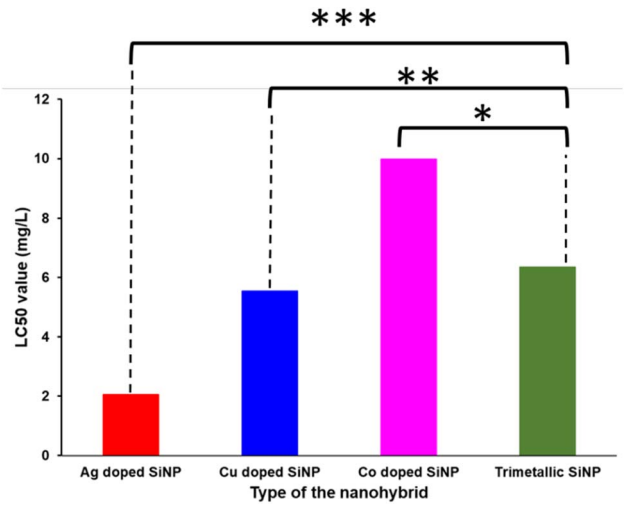

Fig. 4 The statistical analysis between monometallic SiNPs and trimetallic SiNPs; * the significant difference between the LC_{50} values of trimetallic SiNPs and CoSiNPs, *** the significant difference between the LC_{50} values of trimetallic SiNPs and CuSiNPs, and *** the significant difference between the LC_{50} values of trimetallic SiNPs and AgSiNPs.

3.4 Calculating the cumulative apical points of the ZFET assay

The assessment of nanohybrid developmental toxicity included calculations based on Zebrafish Embryo Test (ZFET) assay apical endpoints that were accumulated throughout the testing period of 96 hours. The evaluation of impact of nanohybrids on early developmental stages utilizes these four apical endpoints: coagulation of the embryo, failure of somite formation, non-detected tail, and absence of heartbeat. The observations in the ZFET assay included the four synthesized types of nanohybrids at various concentrations ranging from 10.000 mg L^{-1} to 0.156 mg L^{-1}, and were recorded at time intervals of 24 hours, 48 hours, 72 hours, and 96 hours. During these time points, the developmental stages of the embryos were closely monitored. To provide a visual representation of the overall observations, photographs of the growing embryos were captured. Fig. 6 highlights some significant observations from the AgSiNP sample, showcasing key developmental effects observed at different concentrations and time intervals.

A substantial number of embryos developed coagulation at the highest concentration tested, which stood at 10 mg L^{-1}, as shown in Fig. 5. Embryonic coagulation occurs when the yolk or complete embryo starts clumping because severe developmental arrest blocks growth and developmental advancement. Embryonic developmental failures and possible mortality become evident when normal embryonic processes are disrupted by high nanoparticle concentrations. The strong toxicity of higher nanoparticle concentrations emerges from this experimental result during early development.

A decrease in nanohybrid concentration resulted in reduced embryo developmental abnormalities because of dosage effects. The embryos revealed less toxic impacts when the nanohybrid

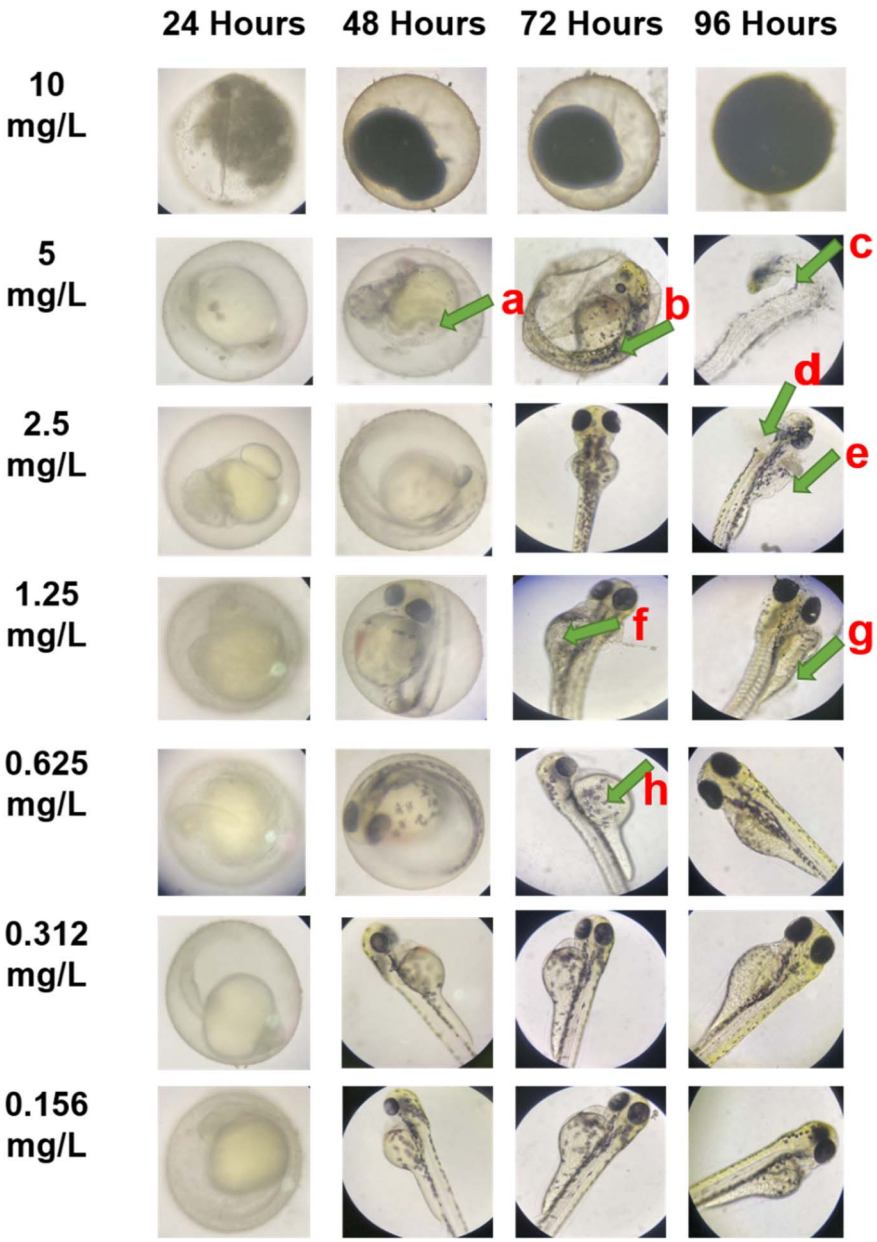

Fig. 5 Developmental abnormalities observed in zebrafish embryos exposed to varying concentrations (10–0.156 mg L^{-1}) of the synthesized AgSiNPs at different time intervals (24, 48, 72, and 96 hours).

concentration was lowered because they displayed fewer apical points in reduced numbers. Lower nanohybrid exposure levels enhance normal embryonic development by causing limited adverse effects on vital developmental operations.

Analysis of Fig. 5 verifies the observation of delayed egg hatching that occurred when concentrations increased. Embryonic development failed to progress normally as cell division and organogenesis influenced hatching times for exposed embryos. The time to embryo hatching showed maximum delay at higher toxicant concentrations, thus confirming that the toxicant affected embryo development according to its concentration levels.

Various developmental abnormalities, apart from delayed hatching, became evident as part of the observed results. One of the principal abnormalities recorded by researchers was the inability of tails to detach from the embryo (Fig. 5 shows this defect as (a)). The intriguing part of the experiment is that the tail failed to secede from the tailbud, thus disrupting the neuromuscular system and somatic mesoderm development. A defective tail points to problems during the development of muscles and nervous system structures, which are vital for normal motor function.

The creation of somites failed to occur during early embryonic development, as shown by anomaly (b) in Fig. 5. Somites arise from mesodermal embryonic tissue and function to build the vertebral column, muscles, and dermis tissues. Missing somites indicate a developmental problem with mesodermal tissues, which results in skeletal defects along with possible

muscle abnormalities. The nanohybrid concentrations caused substantial disruptions to crucial body plan developing structures, which led to this developmental error.

The entire embryo structure experienced a critical failure, as demonstrated in Fig. 5(c), showing a complete breakdown of ectoderm and mesoderm developmental layers. Tissue failure causes the breakdown of developing structures that include the epidermis, muscles, and nervous system, resulting in complete developmental arrest. The severe developmental problem occurs mainly in embryos when they come in contact with high doses of toxic substances such as nanoparticles. A severe tear extended through the hindbrain area. Fig. 5(d) represents an essential element required for cranial nerve development as well as motor control sophistication. Motor dysfunction along with neurological impairment becomes a possibility for individuals when their hindbrain suffers rupture because this important brain region regulates heart rate while managing breathing activities. The abnormal formation confirms that high nanohybrid concentrations generate major neuropathological tissue damage. The data show that the yolk sac experienced a collapsing pattern in a few embryos during evaluation (Fig. 5(e) and (g)). Embryonic growth retardation, followed by death, occurs because the yolk sac provides essential nutrients to embryos but fails in its functions after exposure to the nanohybrids. The development of the embryo often becomes toxic during early stages, when an abnormality indicates it cannot properly take in the necessary nutrients from the yolk.

The presence of pericardial oedema, marked in Fig. 5(f) and (h), in various embryos indicates fluid accumulation around the heart. Cardiotoxicity describes the cardiac system developmental problems that result in this condition. Patients who experience pericardial oedema have severe circulatory function problems because it shows the potential for both vascular leakage and heart failure, affecting basic cardiac development.

The nanohybrids demonstrate significant toxic behavior toward different organ systems, starting from the musculoskeletal system through the nervous system to the vascular and cardiovascular systems, particularly at elevated concentrations. Controlling the concentration level of nanohybrids becomes vital because their developmental toxicity depends on the dosage received. Developmental embryo safety can be achieved through proper nanohybrid exposure management at reduced concentrations since fewer abnormalities occur.

Fig. 6 shows some highlights of the significant observations from the CuSiNP sample, showcasing key developmental effects observed at different concentrations and time intervals. Fig. 6 illustrates the occurrence of coagulation in many embryos because they were exposed to the highest concentration of 10 mg L^{-1}. A severe disruption of embryonic development causes coagulation, which halts the growth process of developing embryos. High concentration coagulation represents toxic effects that stop embryonic development. Outside the highest concentration range of CuSiNPs, fewer development defects occurred due to the dose–response pattern. The embryos exposed to reduced CuSiNP concentrations experienced regular developmental progress since these lower levels did not affect fundamental biological functions.

The hatching process occurred later when embryos were exposed to increased concentrations of CuSiNPs, as depicted in Fig. 6. The delayed hatching period reflects cellular process disorders that affect both cell division and organ development needed for proper zebrafish embryo hatching. The nanohybrids presented toxic effects that delayed essential developmental processes, thus leading to slower embryonic development at higher concentrations.

The most prominent of all observed developmental deformities was caudal flexion, which involved tail bending ((a) in Fig. 6). Neuromuscular development and mobility depend on a functional tail structure. Immunotoxic damage across the tail structure obstructs the development of somites and muscles, which results in restricted movement abilities. A defect caused by mesodermal and neural development disruption is essential for body structure and muscle function.

The researchers noted the absence of somite formation as a major developmental abnormality ((b) in Fig. 6). The proper development of the vertebral column muscles and dermis depends on somite formation. A developmental issue in the mesoderm leads to somite absence because this defect prevents the embryo from forming the necessary skeletal and muscle structures. The mesodermal differentiation appears to be affected by the presence of CuSiNPs, since this defect emerges as a result. The recorded observations documented the occurrence of yolk sac and pericardial ruptures, featured as (c) in Fig. 6. The embryo suffers from major organ destruction, as shown by the observed ruptures. Embryonic survival suffers significant detriment when the yolk sac ruptures because development needs that sac as its main nutritional source for embryo growth. The pericardial rupture reveals cardiac dysregulation because it surrounds the heart tissue, thus potentially resulting in circulatory defects or heart failure.

The presence of yolk sac oedema was also recorded during the examination ((d) in Fig. 6) along with the observed ruptures of yolk sac and pericardium. Embryonic death becomes a serious risk when this oedema persists because it impairs the embryo's ability to absorb nutrients, thus causing growth problems. Although various embryos presented with heart fluid accumulation known as pericardial oedema ((e) in Fig. 6), this demonstrates potential heart toxicity. The vascular abnormality disrupts normal circulatory development while indicating dysfunction of the embryonic vascular system.

Fig. 7 shows some highlights of the significant observations from the CoSiNP sample, showcasing key developmental effects observed at different concentrations and time intervals. The number of apical points decreased substantially in CoSiNPs, which demonstrated that this nanohybrid shows lower toxicity toward zebrafish embryos. This lower toxicity manifests itself through decreased developmental abnormalities as well as through the lowest LC_{50} result across all tested nanohybrids. Safety margins for CoSiNPs exceed those of others, while they do not produce significant developmental abnormalities in the zebrafish embryo population.

The most significant outcome from testing at 10 mg L^{-1} concentration showed that nanoparticles aggregated particularly around the zebrafish embryo and resulted in coagulation

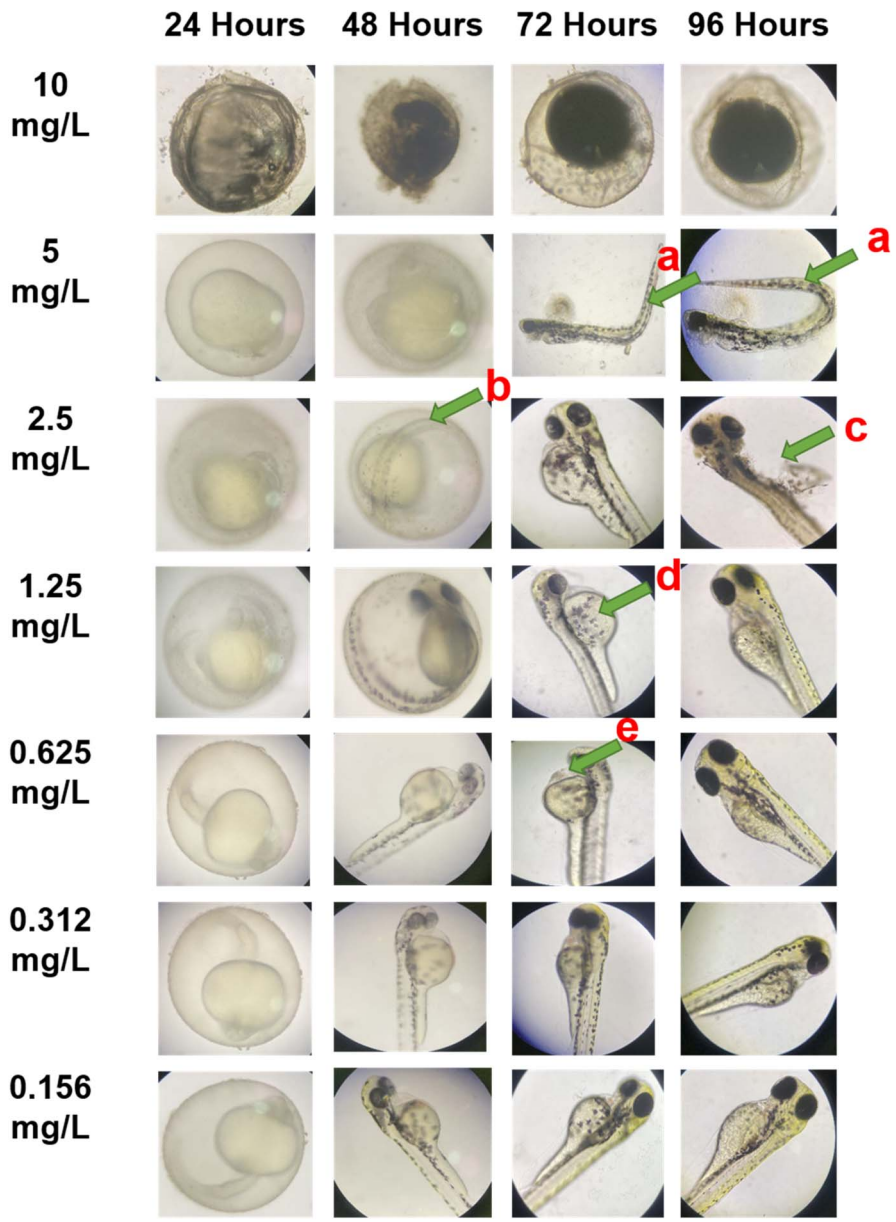

Fig. 6 Developmental abnormalities observed in zebrafish embryos exposed to varying concentrations (10–0.156 mg L^{-1}) of the synthesized CuSiNPs at different time intervals (24, 48, 72, and 96 hours).

(a). Nanohybrids gathered in clusters around the yolk sac and embryonic body according to microscopic observations. Silicon nanoparticles with cobalt doping exhibit adhesive behavior, which causes them to adhere to external embryo surfaces that include the ectoderm along with the yolk sac. Embryonic embryos receive nutrients from their yolk sac reserve, and nanoparticle clusters around this area might impact nutrient absorption, yet no embryos exhibited either rupture or rupture-caused developmental abnormalities at these exposure levels.

Most embryonic developmental issues involved yolk sac oedema, which appeared as (b) in Fig. 7. An accumulation of fluid within the yolk sac indicates both fluid balance disruption and vascular breakdown because of the yolk sac oedema condition. The improper transfer of nutrients from the yolk to the embryo leads to growth reduction while potentially delaying embryo development because of this condition. The number of developmental abnormalities remained lower compared to other nanohybrids, indicating that Co-doped SiNPs show milder toxic conditions than their Ag-doped and Cu-doped along with trimetallic counterparts.

Fig. 8 highlights some significant observations from the trimetallic silica nanohybrid sample, showcasing key developmental effects observed at different concentrations and time intervals.

When exposed to high concentrations of trimetallic SiNPs, the embryos turned into solid masses. The high concentrations of nanoparticles appear to interfere with regular development, causing blood circulation disruption and substantial

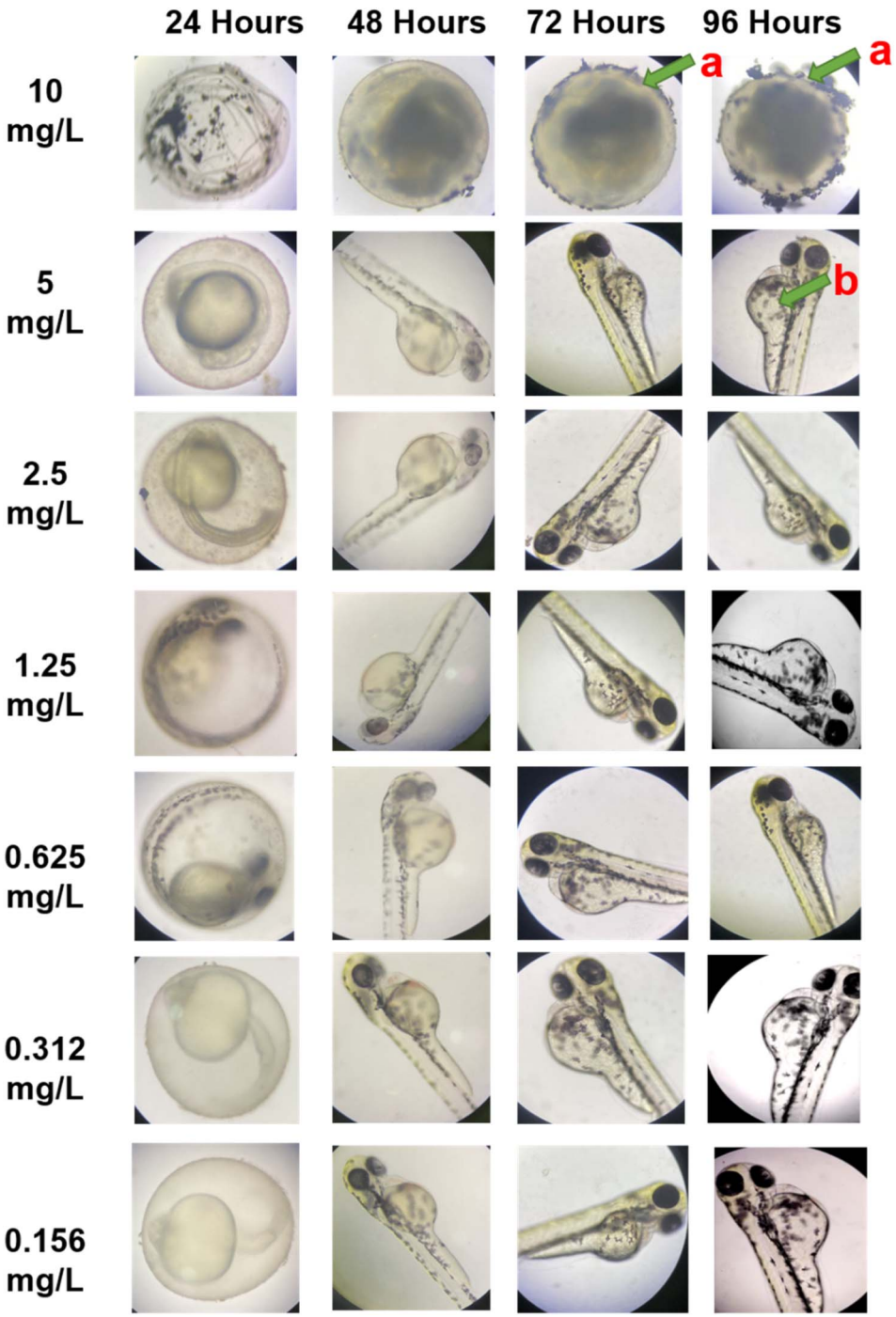

Fig. 7 Developmental abnormalities observed in zebrafish embryos exposed to varying concentrations (10–0.156 mg L^{-1}) of the synthesized CoSiNPs at different time intervals (24, 48, 72, and 96 hours).

deformations. Previous investigations examining CoSiNPs revealed similar findings that showed both coagulation and embryonic development problems. The embryos failed to exhibit additional harmful developmental signs beyond coagulation at both apical points in the trimetallic and CoSiNP tests.

The nanohybrid concentration rise led to the appearance of two distinct pathological attributes. The yolk sac, along with the pericardium showed a torn structure (Fig. 8a). The structural breakdown of essential embryonic membranes seems to result from excessive nanoparticle concentration, which potentially causes major mechanical stress to embryonic structures. Pathological observations revealed the development of yolk sac oedema in embryos that received higher concentrations of nanohybrids because nanoparticles seem to alter normal fluid regulation or produce inflammation within the essential yolk sac structure that nourishes embryonic development.

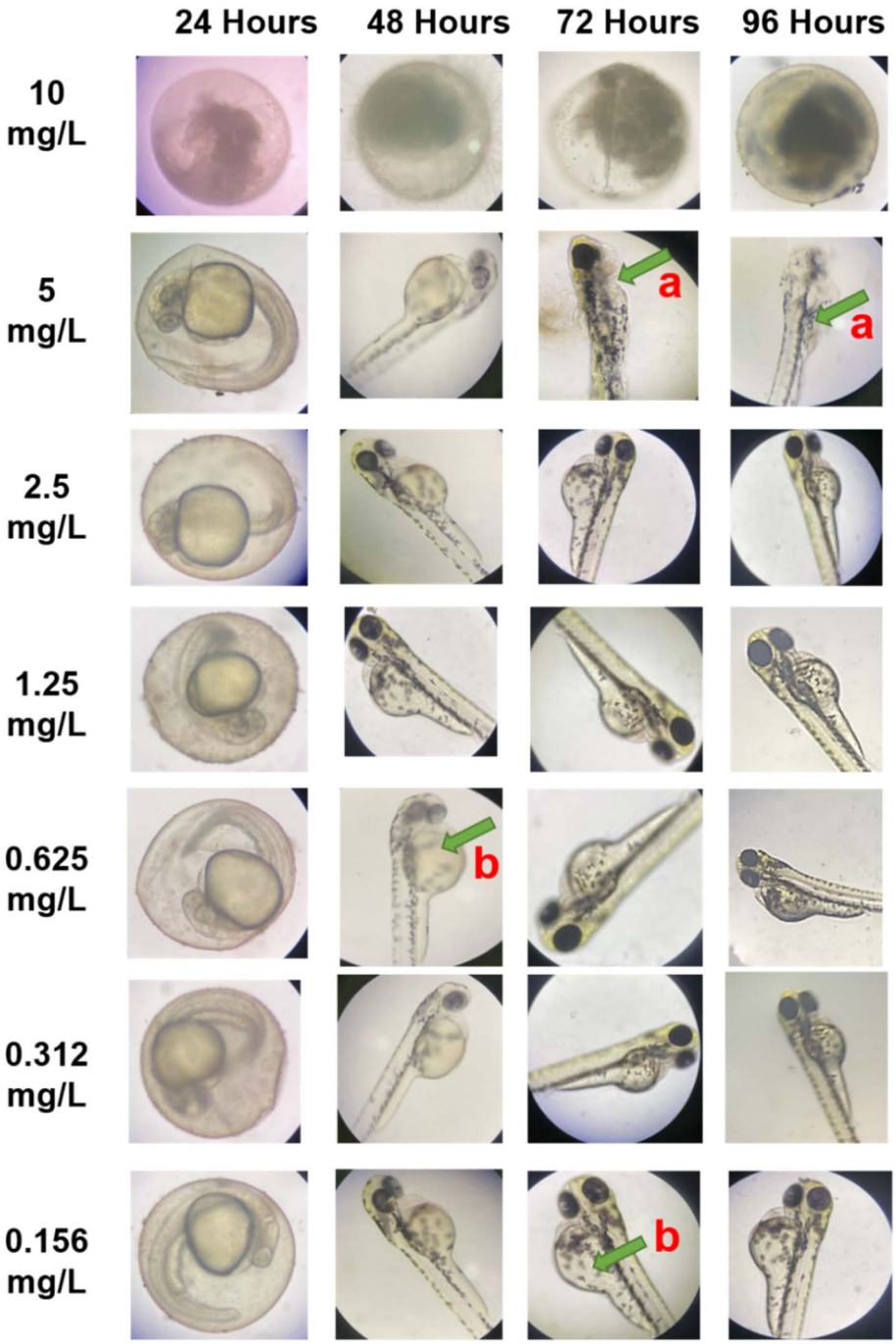

Fig. 8 Developmental abnormalities observed in zebrafish embryos exposed to varying concentrations (10–0.156 mg L^{-1}) of the synthesized trimetallic SiNPs at different time intervals (24, 48, 72, and 96 hours).

The main observation indicated that embryos administered with trimetallic SiNPs hatched on time without experiencing substantial delays compared to the AgSiNP and CuSiNP conditions. Furthermore, the studies indicate that developmental disturbances from trimetallic SiNPs did not prevent normal embryo hatching progression. The AgSiNPs, along with the CuSiNPs, showed longer hatching delay periods than the trimetallic SiNP-exposed embryos. These data imply worse toxicity effects and developmental interferences for AgSiNP and CuSiNPs over the trimetallic SiNPs.

Research data show that trimetallic SiNPs during high concentration exposure led to significant developmental defects such as coagulation alongside yolk sac rupture and oedema however they fail to prolong hatching times. The developmental disturbances observed cannot be attributed to widespread developmental delays, which other nanoparticle formulations have demonstrated.

Following these observations, the percentage of cumulative apical points for each concentration of all the synthesized nanohybrids, including AgSiNPs, CuSiNPs, CoSiNPs, and

Table 4 The percentages of cumulative apical points and the p values calculated by the Wilcoxon signed-rank test

	AgSiNP		CuSiNP		CoSiNP		Trimetallic SiNP	
Concentration (mg L^{-1})	% cumulative apical points	p value	% cumulative apical points	p value	% cumulative apical points	p value	% cumulative apical points	p value
10.00	86.25	0.015	94.58	0.015	94.17	0.015	52.08	0.015
5.00	68.33	0.015	86.67	0.015	64.17	0.015	40.00	0.015
2.50	64.58	0.015	80.83	0.015	63.33	0.058	31.67	0.015
1.25	58.33	0.015	60.00	0.015	52.92	0.058	25.42	0.058
0.625	52.50	0.015	44.17	0.015	38.34	0.058	23.33	0.058
0.312	39.58	0.015	42.50	0.058	26.67	0.058	20.00	0.058
0.156	12.50	0.058	29.58	0.058	13.75	0.084	12.08	0.084

trimetallic SiNPs, was calculated. The cumulative apical points at the end of the 96-hour period were also scored according to the method described in Section 2.2.2. Afterwards, these scores were statistically analyzed by employing the Wilcoxon signed-rank test at a significance level of 0.05. Table 4 shows the percentages of cumulative apical points and the p values calculated by the Wilcoxon signed-rank test based on the observed apical points at the end of the 96 hours.

A cumulative apical points score reached 86.25% ($p = 0.015$) when using 10 mg L^{-1} of AgSiNPs, leading to significant toxic effects. The developmental impact of CuSiNPs became more pronounced as the concentration reached 10 mg L^{-1} because they achieved a cumulative apical point score of 94.58% ($p = 0.015$). The toxic effects of both CoSiNPs and trimetallic SiNPs became apparent at the identical 10 mg per L concentration by causing 94.17% ($p = 0.015$) and 52.08% ($p = 0.015$) cumulative apical points, thus indicating severe developmental impairments in embryos exposed to such nanohybrids.

The effects of nanohybrids at 5 mg L^{-1} presence still caused significant damage to embryos, although developmental defects became less pronounced. At 5 mg per L concentration, AgSiNPs showed 68.33% significant toxicity ($p = 0.015$) however, CuSiNPs demonstrated slightly better effects with 86.67% significant toxicity ($p = 0.015$). The toxicity of CoSiNPs and trimetallic SiNPs remained moderate when examined at this concentration because they presented cumulative apical points totaling 64.17% ($p = 0.015$) and 40.00% ($p = 0.015$), respectively. These nanohybrids maintained strong toxic impacts on zebrafish embryos even at this specific concentration level.

The cumulative apical points remained statistically significant for AgSiNPs and CuSiNPs at 2.50 mg L^{-1} as determined by p-values of 0.015% and 0.015%. The toxicity measurement of CoSiNPs resulted in a modest decline to 63.33% ($p = 0.058$) but maintained borderline significance, while trimetallic SiNPs exhibited a substantial decrease, leading to 31.67% apical points ($p = 0.015$). Dopant concentration still maintains high toxicity between AgSiNPs and CuSiNPs, but decreased toxicity levels are observed in both CoSiNPs and trimetallic SiNPs.

1.25 mg L^{-1} caused an additional reduction in the toxic effects observed. AgSiNPs, along with CuSiNPs, maintained their toxic properties by causing significant effects, leading to 58.33% ($p = 0.015$) and 60.00% ($p = 0.015$) cumulative apical points. The toxicity of CoSiNPs (52.92%, $p = 0.058$) and trimetallic SiNPs (25.42%, $p = 0.058$) proved lower than higher concentration levels, while CoSiNPs demonstrated borderline significance and trimetallic SiNPs displayed substantially diminished toxic effects.

The toxicological effects remained noticeable at 0.625 mg per L. AgSiNPs caused 52.50% ($p = 0.015$) and CuSiNPs caused 44.17% ($p = 0.015$) significant harm. At this concentration, CoSiNPs (38.34%, $p = 0.058$) and trimetallic SiNPs (23.33%, $p = 0.058$) presented marginally important findings, which indicated decreased toxicological effects. Nanohybrids exposed to the lowest concentration level of 0.156 mg L^{-1} resulted in considerable apical point reduction, where AgSiNPs dropped to 12.50% ($p = 0.058$), Cu-doped SiNPs reached 29.58% ($p = 0.058$) and CoSiNPs reduced to 13.75% ($p = 0.084$), and trimetallic SiNPs fell to 12.08% ($p = 0.084$). At this concentration testing, the p-values exceeded 0.05 for both CoSiNPs and trimetallic SiNPs because these concentrations lacked statistical significance, although AgSiNPs and CuSiNPs still produced significant developmental toxicity.

The experimental results show that AgSiNPs and CuSiNPs produced the greatest cumulative apical points at every concentration level, which indicates their toxicity to zebrafish embryos, particularly at elevated concentrations. When used at lower concentrations, CoSiNPs alongside trimetallic SiNPs showed reduced toxicity to zebrafish embryos. The observed toxicological effects are statistically meaningful based on significant p-values at most concentrations however, specific nanohybrid effects diminish to nondetectable levels at decreased doses.

Following the statistical analysis, the observed apical points were analyzed separately. This analysis includes the observations of the four apical points including coagulation of the embryo, lack of somite formation (a somite is an early-stage division of a body part of an embryo that eventually goes on to form vertebrate, skeletal muscle, cartilage, tendons, and skin of the back), non-detachment of the tail and lack of heartbeat. Fig. 9 shows a graphical interpretation of the apical points observed at various concentrations in various nanohybrids.

Different nanohybrids extracted from the zebrafish embryo toxicity assay generated substantial developmental toxicity, which affected AgSiNPs, CuSiNPs, CoSiNPs, and trimetallic SiNPs. The toxic effects changed based on the concentration that each sample contained. The maximum coagulation occurrences of 182 and 171 were recorded when using AgSiNPs

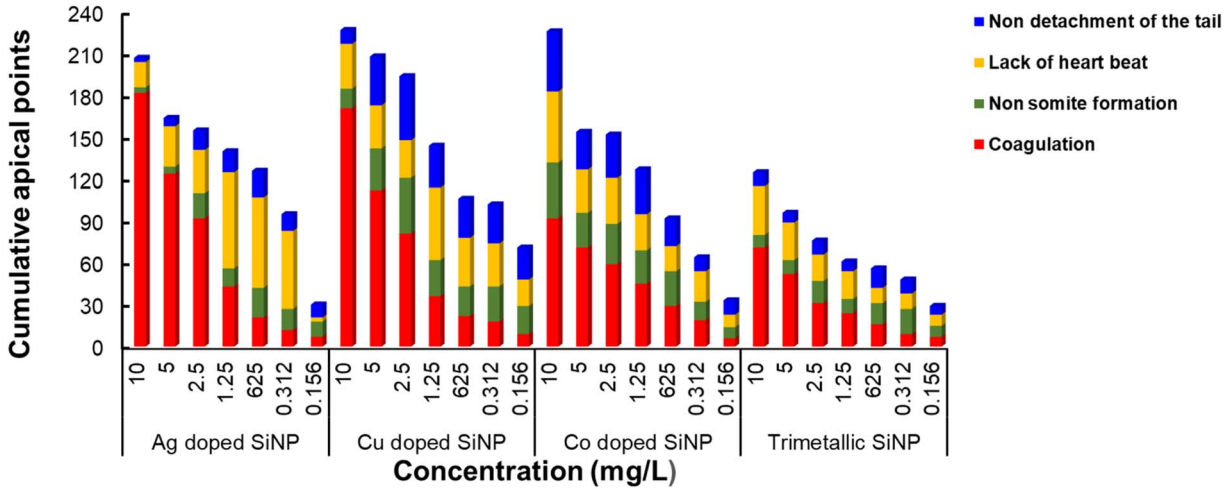

Fig. 9 A graphical interpretation of the apical points observed at various concentrations in various nanohybrids.

and CuSiNPs at a concentration of 10 mg L^{-1}. When the nanohybrids reached higher doses, they displayed substantial toxicity levels that corresponded to the concentration levels, decreasing the coagulation results. The coagulation events remained lower for CoSiNPs coupled with trimetallic SiNPs at a concentration of 10 mg L^{-1} when compared to other nanohybrids, which suggests that these nanohybrids exhibited reduced coagulation potency.

A deficiency in non-somite formation development, which indicates somite segmentation defects, became more common when the embryos received AgSiNPs or CuSiNPs at lower dosage levels. The non-somite formation counts at 2.5 mg L^{-1} reached 18 due to AgSiNPs, but CuSiNPs exhibited 40 cases at 5 mg L^{-1}. Different nanohybrid concentrations dictate how much they endanger embryonic development, according to this study. CoSiNPs and trimetallic SiNPs produced similar developmental disruption effects, but CoSiNPs created 40 non-somite formations at 2.5 mg L^{-1}, whereas trimetallic SiNPs induced 15 such defects at this concentration.

A critical evaluation of developmental toxicity revealed maximum rates of lack of heartbeat at 10 mg L^{-1} concentration by all nanohybrids. The number of non-heartbeat cases during AgSiNPs exposure increased from 18 to 69 when the concentration increased from 10 mg L^{-1} to 1.25 mg L^{-1}, showing increasing abnormality with dosage. The percentage of beatless hearts within the test subjects decreased from 32 cases at 10 mg L^{-1} to 9 cases at 0.156 mg L^{-1} when exposed to Cu-doped SiNPs in a manner that followed the dose–response pattern. The occurrence of absence of heartbeat decreased for CoSiNPs and trimetallic SiNPs as compared to other nanohybrids at equivalent concentration levels.

When exposed to 5 mg L^{-1} of CuSiNPs, the non-detachment of the tail occurred 46 times, indicating developmental problems in the tail region. At 0.156 mg per L concentration, the occurrence of this defect appeared in 10 cases using trimetallic SiNPs and 7 instances with CoSiNPs. The nanohybrids induced tail developmental issues, yet the intense dangers reduced as the concentration levels decreased.

Developmental toxicity analysis shows that AgSiNPs and CuSiNPs possess high toxic effects against embryonic development through their strong impact at elevated concentrations, where they lead to crucial defects such as coagulation, non-somite formation, lack of heart function, and non-detachment of the tail. The embryonic development of zebrafish survived better in Co-doped and trimetallic SiNP solutions despite their toxic nature at higher solution concentrations. Additional studies must analyze the toxicity mechanisms of these nanohybrids because toxicological effects depend on the concentration of nanohybrids and the embryo developmental stage.

Considering the published literature, there were similar studies that reported results of a similar nature. Tiago *et al.* investigated the toxic effects of metformin, sodium metavanadate, and their co-encapsulation in polycaprolactone (PCL) nanoparticles on zebrafish (*Danio rerio*). Acute toxicity tests revealed both lethal and sublethal effects, including pericardial edema, particularly in groups exposed to sodium metavanadate and the nanoparticle formulations. The study found that polycaprolactone in the nanoparticles negatively impacted cardiovascular development, reducing heart rate and causing developmental issues in zebrafish embryos and eleutheroembryos, regardless of concentration. These findings highlight the importance of toxicological evaluations of nanomaterials to identify potential toxicity risks before their use in veterinary applications.[46]

Carbaugh *et al.* developed a high-throughput toxicity screening method using a zebrafish photomotor response (PMR) test to assess the toxicity of fifteen engineered nanomaterials relevant to military applications. The study utilized automated dechorionation to enhance the bioavailability of nanomaterials in zebrafish embryos. Behavioral responses were observed for thirteen of the fifteen nanomaterials, with acute toxicity levels (LC_{50}) identified for nine nanomaterials below the maximum concentration of 500 μg mL^{-1}. The results emphasize the importance of physico-chemical characterization in toxicity testing due to the detected endotoxin and bacterial contamination in some samples.[47]

Moreover, Ortiz-Román *et al.* investigated the ecotoxicological effects of titanium dioxide (TiO_2) P25 nanoparticles on zebrafish embryos and eleutheroembryos, focusing on toxicity levels, hatching rates, embryo development, and TiO_2 accumulation in tissues. Zebrafish embryos were exposed to varying concentrations of TiO_2 NPs for 48 and 96 hours. While mortality and hatching rates were not significantly affected, developmental issues and physical malformations were observed. The study found that the highest concentrations of TiO_2 in zebrafish larvae were 1.0199 mg L^{-1} after 48 hours and 1.2679 mg L^{-1} after 96 hours of exposure. Up to 11% of embryos exhibited physical malformations, suggesting teratogenic effects that could negatively impact the species and aquatic ecosystems.[48]

3.5 Calculating the therapeutic index for each nanohybrid against the tested microorganisms

The therapeutic index (TI) was calculated for each metal-doped silica nanohybrid to assess their relative safety and antimicrobial effectiveness against the tested microorganisms. The TI values were determined by dividing the LC_{50} (obtained from zebrafish embryo assays) by the MIC values (considered equivalent to ED_{50}) for each nanohybrid-microbe combination. The calculated TI values are summarized in Table 5. These results indicate that the trimetallic silica nanohybrid exhibited notably higher TI values across all tested strains, demonstrating its enhanced balance of antimicrobial efficacy and reduced toxicity compared to the monometallic variants.[36]

The calculated therapeutic indices reveal clear differences in the safety–efficacy balance among the tested nanohybrids. The trimetallic silica nanohybrid consistently demonstrated the highest TI values across all bacterial and fungal strains tested, indicating that it achieves potent antimicrobial activity at lower effective concentrations while maintaining comparatively lower toxicity levels. This suggests that the combined action of Ag, Cu, and Co within a single silica matrix generates a synergistic effect that enhances antimicrobial potency without proportionally increasing toxicity. In contrast, the monometallic nanohybrids showed lower TI values, especially for CoSiNPs, which indicates that higher concentrations are required to achieve comparable antimicrobial effects, narrowing their safety margin. Overall, these results emphasize that the nanoarchitectonic approach of integrating multiple metal dopants into a single nanohybrid not only improves antimicrobial effectiveness but also broadens the therapeutic window, making the trimetallic nanohybrid a more promising candidate for safe and effective antimicrobial applications.

Table 5 Calculated therapeutic index (TI) values for each metal-doped silica nanohybrid against the tested microorganisms

Microbe	AgSiNP	CuSiNP	CoSiNP	Trimetallic silica nanohybrid
S. aureus	21.13	28.07	12.81	259.18
S. pneumoniae	41.84	28.07	12.81	259.18
MRSA	21.13	28.07	12.81	259.18
E. coli	21.13	28.07	6.40	259.18
K. pneumoniae	10.40	28.07	6.40	129.59
P. aeruginosa	10.40	28.07	6.40	129.59
C. albicans	21.13	28.07	12.81	259.18
T. rubrum	41.84	28.07	12.81	259.18
M. gypseum	21.13	28.07	12.81	259.18
A. niger	21.13	28.07	6.40	259.18

3.6 Assessing the skin irritation potential of metallic silica nanohybrids and the electrospun polymer mat incorporated with trimetallic silica nanohybrid by the HET-CAM assay

According to the methodology described in Section 2.2.3, the observations of the hen's egg test-chorioallantoic membrane assay were recorded when exposed to the synthesized nanohybrid samples and scored. Table 6 shows the irritation scores of the various nanohybrid samples.

The HET-CAM assay results show that different nanohybrids tend to irritate tissues more or less than negative control substances and positive control irritants. This assay assigns materials irritancy rankings according to their effects through experimental scores analyzed under ICCVAM guidelines, where ratings from 0 to 9 define non-irritating materials, yet scores from 10 to 21 show irritancy. Analysis reveals that AgSiNPs possess an irritation score of 13.33 ± 0.58 based on the ICCVAM protocol for classification, thus defining it as "irritating". The irritation from silver-doped SiNP formulations remains at moderate levels, thus affecting their suitability in biomedical settings, assuming direct contact occurs between particles and ocular tissues.

The irritant classification is also valid for CuSiNPs due to their test score of 11.67 ± 0.58. Medical applications involving sensitive tissue contact with copper-doped SiNPs reveal an increased potential for irritation based on the test results. The assay results for CoSiNPs show non-irritant characteristics with a score of 1.00 ± 1.00. Cobalt-doped SiNPs exhibit lower rates of irritation, thus making them a suitable candidate for biomedical applications that require high biocompatibility and minimal tissue irritation.

The trimetallic SiNPs have a test result of 3.67 ± 0.58, which places them in the non-irritating group. The findings regarding the SiNPs containing three metal components are significant because they demonstrate minimal inflammatory or irritative capabilities, which present a favorable outlook for biomedical and therapeutic applications requiring contact with sensitive biological tissues. The test solution in 0.9% NaCl received a score of 0.00 ± 0.00 as the negative control, while the positive control (0.1 N NaOH) earned a score of 19.67 ± 0.58. The negative control revealed no skin irritation through the assay,

Table 6 The irritation scores of the various nanohybrid samples

Nanohybrid	Irritation score	Irritant or not
AgSiNP	13.33 ± 0.58	Irritant
CuSiNP	11.67 ± 0.58	Irritant
CoSiNP	1.00 ± 1.00	No
Trimetallic SiNP	3.67 ± 0.58	No
Negative control (0.9% NaCl)	0.00 ± 0.00	No
Positive control (0.1 N NaOH)	19.67 ± 0.58	Irritant

while the positive control confirmed the highly irritating properties of 0.1 N NaOH.

Nanohybrids consisting of SiNPs and Ag or Cu demonstrate moderate levels of irritation, yet nanohybrids that contain Co or the trimetallic combination do not produce irritation. These findings provide crucial knowledge for selecting suitable materials when designing biomedical systems that need both reduced skin irritation and enhanced compatibility with biological systems. Fig. 10 shows significant observations that were observed during the experiment.

A two-sample *t*-test analyzed the irritation scores between the monometallic nanohybrids and the trimetallic nanohybrid, considering the negative control at a 0.05 significance level. All nanohybrids demonstrated significant differences when compared to the negative control, which proved their capability to cause increased skin irritation *versus* the 0.9% NaCl solution. These materials show some irritation capabilities according to this finding; however, laboratory data alone cannot precisely determine their impact on advanced biological systems.

When analyzing the published literature on the HET-CAM assay related to nanomaterials, Smail *et al.* conducted a study evaluating the *ex vivo* irritation potential of a novel brimonidine nanoemulsion using the Hen's Egg Test on Chorioallantoic Membrane (HET-CAM) assay. The HET-CAM method assesses the irritant potential of substances in an *ex vivo* setting. The results indicated that brimonidine nanoemulsions exhibited non-irritating potential when compared to conventional eye drops.[49]

Yadav *et al.* conducted a study on the cytotoxic evaluation of silver nanoparticles synthesized from green tea extract using the Hen's Egg Test on Chorioallantoic Membrane (HET-CAM) assay and an antimicrobial assay. The results demonstrated that the green tea-synthesized silver nanoparticles exhibited strong antimicrobial effects. Additionally, the nanoparticles were found to be non-irritant according to the HET-CAM assay.[50]

Moreover, Abdurrahman Öztürk *et al.* studied ketorolac tromethamine (KT) loaded nano-spray dried nanoparticles (KT-NPs) for wound healing and anti-inflammatory treatment. The study demonstrated that the nanoparticles showed a monodisperse size distribution and positive zeta potential. KT-NPs significantly enhanced fibroblast proliferation and collagen gene expression (COL1A1), indicating effective wound healing and anti-inflammatory activity. The nanoparticles improved drug delivery and anti-inflammatory effects. Successful results were observed in cell viability and gene expression assays, while the *in vivo* HET-CAM assay confirmed the anti-inflammatory activity of the formulation.[51]

Our choice of the trimetallic silica nanohybrid material was made based on test results when integrating it through electrospinning into polymer membranes. The trimetallic silica nanohybrid exhibited the highest antimicrobial activity, low LC_{50} value, and reduced irritant effects compared to monometallic nanohybrids; hence, it was regarded as an optimal compound for progression. Cellulose acetate (CA) with a molecular weight of 100 kDa was used to fabricate electrospun membranes. For the preparation of the trimetallic nanohybrid-incorporated CA membrane, 600 mg of CA was dissolved in a solvent mixture of acetone and dimethylformamide (DMF) at a volume ratio of 2 : 1. Subsequently, 600 mg of the synthesized trimetallic silica nanohybrid was added to the polymer solution, and the mixture was sonicated for 5 hours at room temperature to ensure uniform dispersion. The resulting solution was electrospun using a static collector plate under ambient conditions with a voltage of 16 kV, a tip-to-collector distance of 13 cm, and a flow rate of 1.5 mL h^{-1}. The fibers were collected on aluminum foil covering the grounded collector plate, producing the trimetallic silica nanohybrid incorporated CA mat. Additionally, ESI 1† shows a confirmation for the presence and homogeneous distribution of each metal throughout the electrospun mat.[5] Furthermore, the antimicrobial efficacy and the associated morphological changes in both bacteria and fungi treated with this trimetallic silica nanohybrid incorporated CA mat have been comprehensively demonstrated in our previous study,[5] confirming their significant antimicrobial potential.

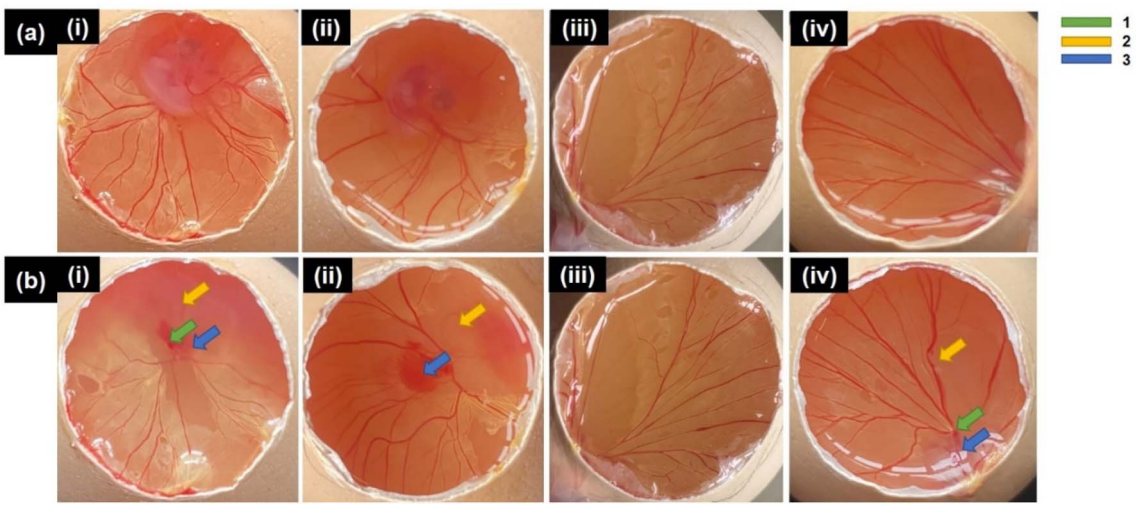

Fig. 10 (a) Before and (b) after exposure to the test substances; (i) AgSiNPs, (ii) CuSiNPs, (iii) CoSiNPs, and (iv) trimetallic SiNPs; (1) coagulation, (2) lysis, and (3) hemorrhages.

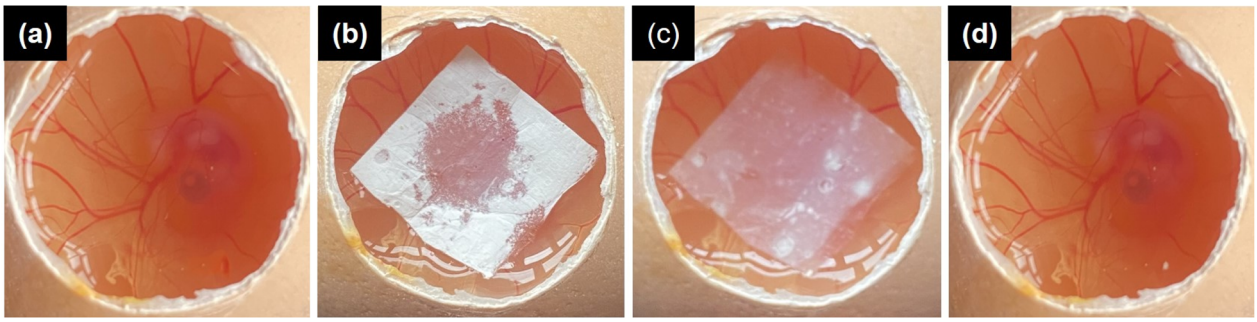

Fig. 11 The observations of (a) before exposure to the trimetallic SiNP-incorporated CA mat; (b) and (c) after applying the trimetallic SiNP-incorporated CA mat; (d) after the removal of the trimetallic SiNP-incorporated CA mat.

In a further modification of the HET-CAM assay, a 4 cm^2 section of a cellulose acetate (CA) mat incorporated with the trimetallic SiNPs was applied to the CAM. This innovative approach aimed to evaluate the irritation potential of a final product designed for potential biomedical applications, such as wound healing and skin contact materials, such as PPE, diapers, sanitary napkins, *etc.* The parameters of interest (hemorrhages, lysis, and coagulations) were meticulously recorded. Remarkably, no signs of irritation were observed in response to the CA mat incorporated with trimetallic SiNPs, indicating excellent biocompatibility and skin compatibility of the material. Fig. 11 shows the observations of the experiment.

However, this HET-CAM assay is not usually recommended for testing the irritating potential of ultra-thin fiber membranes. The testing process should not be treated as a conclusion regarding material safety and biocompatibility, since further analyses are needed to provide definitive results. The assessment using modified HET-CAM holds worth; however, it functions as a primary evaluation approach. Scientific experts around the world recognize that the HET-CAM assay underwent modifications to mirror *in vivo* tests, thus making it an initial screening method before complete animal testing. Complex animal studies will be needed to confirm the testing results obtained under laboratory conditions; therefore, researchers can gain precise knowledge about material effects on whole living organisms. The HET-CAM assay generates useful information, yet a complete assessment needs *in vivo* testing to get a full picture of the safety performance of the nanohybrids for medical purposes.

3.7 Evaluating the skin penetration of the fabricated trimetallic SiNP-incorporated nanofiber membrane

According to the method explained in Section 2.2.4, the skin penetration potential was tested by using a Franz diffusion cell apparatus. Table 7 shows the results of the diffusion assay.[52–54] The results of the Franz diffusion assay, which measured ion release at two-time intervals—6 and 12 hours—provide critical information regarding the release profile of silver (Ag), copper (Cu), and cobalt (Co) ions from the trimetallic SiNPs incorporated into the electrospun membrane. This assay helps us understand how these nanoparticles behave when incorporated into a membrane intended for use in various biomedical applications, such as personal protective equipment (PPE), diapers, sanitary napkins, pampers, and wound dressings. The assay measures the concentration of these metals in the receiving medium, with the levels of Ag, Cu, and Co detected using ICP-MS (Inductively Coupled Plasma Mass Spectrometry). This technique allows for the precise quantification of ion release over time, offering insight into the potential release rates of these ions and their possible biological impact.

Table 7 The diffusion of metals through the Franz diffusion cell; based on ICP-MS analysis

	Concentration (ppm) based on ICP-MS results					
	With the trimetallic SiNP incorporated electrospun membrane			Without the trimetallic SiNP incorporated electrospun membrane		
Time interval (hours)	Ag	Cu	Co	Ag	Cu	Co
6	0.23	0.00	0.00	0.00	0.00	0.00
12	0.26	0.00	0.00	0.00	0.00	0.00

At both the 6-hour and 12-hour time points, the membrane incorporating trimetallic SiNPs released detectable concentrations of silver (Ag), but there was no detectable release of copper (Cu) or cobalt (Co) ions. Specifically, the concentration of Ag at 6 hours was 0.23 ppm, and this increased slightly to 0.26 ppm at the 12-hour mark. These low concentrations of Ag suggest a controlled, slow release of silver ions over time. This is important for biomedical applications, where prolonged or sustained release of active agents such as silver may provide desired antimicrobial properties without overwhelming surrounding tissues. The lack of detectable release of copper and cobalt within the first 12 hours suggests that these metals are either not leaching from the membrane or are doing so at extremely low, undetectable levels under the experimental conditions.

In contrast, the control membrane, which did not contain trimetallic SiNPs, showed no detectable release of silver, copper, or cobalt at either time point. This absence of ion release from the control membrane reinforces the idea that the ion release observed from the membrane containing the trimetallic SiNPs is specifically attributed to the presence of these nanoparticles.

This is a key finding because it suggests that the nanoparticles themselves are responsible for the ion release, which is vital when considering the membrane's function in biomedical applications.

The fabrication of such membranes with low or minimal penetration of metal ions is crucial in the context of biomedical applications. For instance, in products such as PPE, wound dressings, diapers, sanitary napkins, and Pampers, the potential for prolonged contact with the skin or mucous membranes necessitates careful consideration of the release profile of any incorporated materials. It is essential that these materials exhibit minimal or controlled penetration of potentially harmful substances to ensure safety and avoid toxicity. The results from the Franz diffusion assay suggest that the release of silver from the electrospun membrane is limited, which reduces the potential risk of toxicity associated with higher concentrations of silver ions.

This controlled release is particularly important in materials designed for extended use, such as in wound dressings or diapers, where a high penetration of metal ions could lead to adverse effects, including irritation or systemic toxicity. Notably, the levels of silver released from the membrane are still well below the lethal concentration 50 (LC_{50}) values typically associated with silver toxicity, meaning that the amount of silver released is within safe limits for the intended applications. The observed silver concentration (0.23–0.26 ppm) over the first 12 hours is relatively low, suggesting that it remains under the threshold required to induce toxic effects. This provides reassurance that the electrospun membrane can deliver the desired antimicrobial benefits of silver without posing significant risks to users or patients.

In conclusion, while the Franz diffusion assay has provided valuable early-stage data, showing that silver ions are released in a controlled manner, further long-term studies and *in vivo* testing are necessary to fully evaluate the material's performance and safety over extended periods of use in biomedical settings. However, the fact that the release levels of silver remain below toxic thresholds and that the membrane exhibits minimal ion penetration is a promising feature for its incorporation into products that require sustained contact with sensitive tissues or skin.

4 Conclusion

In conclusion, this study successfully evaluated the toxicity and safety profile of a novel nanofiber membrane reinforced with multimetallic silica nanohybrids for potential dermatological applications. The zebrafish embryo toxicity assay revealed that the multimetallic silica nanohybrid had an LC_{50} value of 6.35 mg L^{-1}, which was lower than those of the individual monometallic silica nanohybrids, with LC_{50} values of 2.05 mg L^{-1} for AgSiNPs, 5.53 mg L^{-1} for CuSiNPs, and 9.99 mg L^{-1} for CoSiNPs. This indicates that the multimetallic nanohybrid formulation exhibited reduced toxicity compared to its monometallic counterparts.

The HET-CAM assay showed irritation scores of 13.33 ± 0.58 for AgSiNPs, 11.67 ± 0.58 for CuSiNPs, 1.00 ± 1.00 for CoSiNPs, and 3.67 ± 0.58 for the multimetallic silica nanohybrid. The irritation score for the multimetallic nanohybrid was below the irritant threshold (10–21) according to the ICCVAM protocol, indicating no significant irritation potential ($p = 0.05$). This result suggests that incorporating the metal nanosystems into a non-toxic polymer membrane significantly reduces the potential for skin irritation compared to the monometallic nanohybrids.

Additionally, the Franz diffusion assay revealed that the electrospun membrane containing the multimetallic silica nanohybrid released detectable silver (Ag) ions at a concentration of 0.26 mg L^{-1} after 24 hours, with no detectable copper (Cu) or cobalt (Co) release. Importantly, this released silver concentration was well below the LC_{50} value for Ag, suggesting that the diffusion of silver ions remained at non-toxic levels. The absence of copper and cobalt ion release further supports the reduced toxicity of the multimetallic formulation.

These findings indicate that combining the monometallic nanohybrids into a multimetallic system and incorporating them into a polymer matrix reduces the toxicity and irritation effects typically associated with individual metal nanoparticles. The multimetallic silica nanohybrid-based membrane demonstrated the highest antimicrobial potential, minimal skin irritation, low metal ion diffusion, and a favorable toxicity profile, making it a promising candidate for biomedical applications such as wound dressings, PPE, and other dermatological products. Given these encouraging results, further *in vivo* studies are recommended to confirm the long-term safety and therapeutic potential of this nanofiber membrane.

Ethical statement

According to OECD guideline 236 for the embryo toxicity test, zebrafish embryos are not classified as protected animals within the first 96 hours post-fertilization, as their sensory organs have not yet developed. Therefore, our study, which involved observing zebrafish embryos and larvae for a maximum of 96 hours, fully adheres to these guidelines and does not require ethical approval. Additionally, since the study only involved zebrafish embryos and larvae in their early developmental stages, there were no live animals subjected to procedures that would necessitate euthanasia during the study period. As a precautionary measure, the embryos were humanely euthanized after the completion of the study using an overdose of tricaine methane sulfonate (MS-222), a widely accepted and approved method for euthanasia. However, we emphasize that euthanasia was not required during the study, as it was conducted on embryos and larvae within the first 96 hours of development.

Data availability

All the data are included in this manuscript.

Author contributions

Piumika Yapa – conduct experiments, formal analysis of data and writing the manuscript. Mayuri Geethanjali

Thammitiyagodage – writing the manuscript, data interpretation, methodology, supervision, review and editing the original draft. Imalka Munaweera – conceptualization, funding acquisition, methodology, supervision, writing, review and editing the original draft. All authors have given approval to the final version of the manuscript.

Conflicts of interest

The authors declare that there is no conflict of interest.

Acknowledgements

The authors acknowledge financial support for this study from the University of Sri Jayewardenepura, Sri Lanka.

References

1 A. Haleem, M. Javaid, R. P. Singh, S. Rab and R. Suman, Applications of nanotechnology in medical field: a brief review, *Global Health J.*, 2023, **7**(2), 70–77, DOI: **10.1016/j.glohj.2023.02.008**.

2 S. Wahab, A. Salman, Z. Khan, S. Khan, C. Krishnaraj and S.-I. Yun, Metallic nanoparticles: a promising arsenal against antimicrobial resistance-unraveling mechanisms and enhancing medication efficacy, *Int. J. Mol. Sci.*, 2023, **24**(19), 14897, DOI: **10.3390/ijms241914897**.

3 G. Muteeb, Nanotechnology-a light of hope for combating antibiotic resistance, *Microorganisms*, 2023, **11**(6), 1489, DOI: **10.3390/microorganisms11061489**.

4 M. E. A. de Kraker, A. J. Stewardson and S. Harbarth, Will 10 million people die a year due to antimicrobial resistance by 2050?, *PLoS Med.*, 2016, **13**(11), e1002184, DOI: **10.1371/journal.pmed.1002184**.

5 P. Yapa, I. Munaweera, M. M. Weerasekera and L. Weerasinghe, Synergistic antimicrobial nanofiber membranes based on metal incorporated silica nanoparticles as advanced antimicrobial layers, *RSC Adv.*, 2024, **14**(46), 33919–33940, DOI: **10.1039/d4ra05052e**.

6 P. Yapa, I. Munaweera, M. M. Weerasekera, L. Weerasinghe and C. Sandaruwan, Potential antifungal applications of heterometallic silica nanohybrids: a synergistic activity, *Biomater. Adv.*, 2024, **162**(213930), 213930, DOI: **10.1016/j.bioadv.2024.213930**.

7 K. Ranathunga, P. Yapa, I. Munaweera, M. M. Weerasekera and C. Sandaruwan, Preparation and characterization of Fe–ZnO cellulose-based nanofiber mats with self-sterilizing photocatalytic activity to enhance antibacterial applications under visible light, *RSC Adv.*, 2024, **14**(26), 18536–18552, DOI: **10.1039/d4ra03136a**.

8 S. E. Peiris, K. L. Seneviratne, R. P. A. Shashikala, C. N. Peiris, M. I. Imalka and Y. P. Piumika, In vitro evaluation of antibacterial activity of copper and sulfur nanoparticles for controlling bacterial blight caused by Xanthomonas sp. in Anthurium andraeanum Lind, *SLIIT J Hum & Sci.*, 2022, **3**(1), 46–55.

9 I. P. Madhushika, P. Yapa, I. Munaweera, C. Sandaruwan and M. M. Weerasekera, The antimicrobial synergy of polymer based nanofiber mats reinforced with antioxidants intercalated layered double hydroxides as a potential active packaging material, *Nano Express*, 2024, **5**(2), 025018, DOI: **10.1088/2632-959x/ad4a95**.

10 P. N. Yapa, I. Munaweera, C. Sandaruwan, L. Weerasinghe and M. M. Weerasekera, Metal doped silica nanohybrids with extensive bacterial coverage for antibacterial applications exhibit synergistic activity, *Biomater. Adv.*, 2024, **157**, 213753, DOI: **10.1016/j.bioadv.2023.213753**.

11 I. Munaweera and P. Yapa, *Principles and Applications of Nanotherapeutics*, Taylor & Francis, London, England, 2024.

12 P. N. Yapa, I. Munaweera, M. M. Weerasekera and L. Weerasinghe, Nanoarchitectonics for synergistic activity of multimetallic nanohybrids as a possible approach for antimicrobial resistance (AMR), *J. Biol. Inorg. Chem.*, 2024, **29**(5), 477–498, DOI: **10.1007/s00775-024-02066-w**.

13 S. Selvaraj, M. Perera, P. Yapa, I. Munaweera, I. C. Perera, T. Senapathi, *et al.*, In vitro analysis of XLAsp-P2 peptide loaded cellulose acetate nanofiber for wound healing, *J. Pharm. Sci.*, 2024, **114**(2), 911–922, DOI: **10.1016/j.xphs.2024.10.050**.

14 S. Rajapaksha, P. Yapa and I. Munaweera, Innovation management and nanotechnology: a PRISMA-based analysis and research implications, *Int. J. Innov. Sci.*, 2025, **1**, DOI: **10.1108/ijis-08-2024-0215**.

15 I. Khan, K. Saeed and I. Khan, Nanoparticles: properties, applications and toxicities, *Arab. J. Chem.*, 2019, **12**(7), 908–931, DOI: **10.1016/j.arabjc.2017.05.011**.

16 M. Wang, S. Li, Z. Chen, J. Zhu, W. Hao, G. Jia, *et al.*, Safety assessment of nanoparticles in food: current status and prospective, *Nano Today*, 2021, **39**(101169), 101169, DOI: **10.1016/j.nantod.2021.101169**.

17 L. Xuan, Z. Ju, M. Skonieczna, P.-K. Zhou and R. Huang, Nanoparticles-induced potential toxicity on human health: applications, toxicity mechanisms, and evaluation models, *MedComm*, 2023, **4**(4), e327, DOI: **10.1002/mco2.327**.

18 A. Manke, L. Wang and Y. Rojanasakul, Mechanisms of nanoparticle-induced oxidative stress and toxicity, *BioMed Res. Int.*, 2013, **2013**, 942916, DOI: **10.1155/2013/942916**.

19 C. Egbuna, V. K. Parmar, J. Jeevanandam, S. M. Ezzat, K. C. Patrick-Iwuanyanwu, C. O. Adetunji, *et al.*, Toxicity of nanoparticles in biomedical application: nanotoxicology, *J. Toxicol.*, 2021, **2021**, 9954443, DOI: **10.1155/2021/9954443**.

20 R. K. Shukla, A. Badiye, K. Vajpayee and N. Kapoor, Genotoxic potential of nanoparticles: structural and functional modifications in DNA, *Front. Genet.*, 2021, **12**, 728250, DOI: **10.3389/fgene.2021.728250**.

21 R. Abbasi, G. Shineh, M. Mobaraki, S. Doughty and L. Tayebi, Structural parameters of nanoparticles affecting their toxicity for biomedical applications: a review, *J. Nanopart. Res.*, 2023, **25**(3), 43, DOI: **10.1007/s11051-023-05690-w**.

22 K. Öztürk, M. Kaplan and S. Çalış, Effects of nanoparticle size, shape, and zeta potential on drug delivery, *Int. J. Pharm.*, 2024, **666**(124799), 124799, DOI: **10.1016/j.ijpharm.2024.124799**.

23 J. Thomas, V. Kumar, N. Sharma, N. John, M. Umesh, L. Kumar Dasarahally Huligowda, *et al.*, Recent approaches in nanotoxicity assessment for drug delivery applications: challenges and prospects, *Med. Drug Discovery*, 2025, **25**(100204), 100204, DOI: **10.1016/j.medidd.2025.100204**.

24 R. Akçan, H. C. Aydogan, M. Ş. Yildirim, B. Taştekin and N. Sağlam, Nanotoxicity: a challenge for future medicine, *Turk. J. Med. Sci.*, 2020, **50**(4), 1180–1196, DOI: **10.3906/sag-1912-209**.

25 D. W. Grainger, Nanotoxicity assessment: all small talk?, *Adv. Drug Deliv. Rev.*, 2009, **61**(6), 419–421, DOI: **10.1016/j.addr.2009.04.003**.

26 X. Cheng, Q. Xie and Y. Sun, Advances in nanomaterial-based targeted drug delivery systems, *Front. Bioeng. Biotechnol.*, 2023, **11**, 1177151, DOI: **10.3389/fbioe.2023.1177151**.

27 F. Farjadian, A. Ghasemi, O. Gohari, A. Roointan, M. Karimi and M. R. Hamblin, Nanopharmaceuticals and nanomedicines currently on the market: challenges and opportunities, *Nanomedicine*, 2019, **14**(1), 93–126, DOI: **10.2217/nnm-2018-0120**.

28 S. Zhang, L. Lin, X. Huang, Y.-G. Lu, D.-L. Zheng and Y. Feng, Antimicrobial properties of metal nanoparticles and their oxide materials and their applications in oral biology, *J. Nanomater.*, 2022, **2022**(1), 1–18, DOI: **10.1155/2022/2063265**.

29 R. Singla, A. Guliani, A. Kumari and S. K. Yadav, Metallic nanoparticles, toxicity issues and applications in medicine, in *Nanoscale Materials in Targeted Drug Delivery, Theragnosis and Tissue Regeneration*, Springer Singapore, Singapore, 2016, pp. 41–80.

30 E. Haque and A. C. Ward, Zebrafish as a model to evaluate nanoparticle toxicity, *Nanomaterials*, 2018, **8**(7), 561, DOI: **10.3390/nano8070561**.

31 L. Y. Rizzo, S. K. Golombek, M. E. Mertens, Y. Pan, D. Laaf, J. Broda, *et al.*, In vivo nanotoxicity testing using the zebrafish embryo assay, *J. Mater. Chem. B*, 2013, **1**(32), 3918, DOI: **10.1039/C3TB20528B**.

32 A. Batista-Duharte, G. J. Murillo, U. M. Pérez, E. N. Tur, D. F. Portuondo, B. T. Martínez, *et al.*, The hen's egg test on chorioallantoic membrane: an alternative assay for the assessment of the irritating effect of vaccine adjuvants: an alternative assay for the assessment of the irritating effect of vaccine adjuvants, *Int. J. Toxicol.*, 2016, **35**(6), 627–633, DOI: **10.1177/1091581816672187**.

33 R. C. Hubrecht and E. Carter, The 3Rs and Humane Experimental Technique: Implementing Change, *Animals*, 2019, **9**(10), 754, DOI: **10.3390/ani9100754**.

34 L. M. Schechtman, Implementation of the 3Rs (refinement, reduction, and replacement): validation and regulatory acceptance considerations for alternative toxicological test methods, *ILAR J.*, 2002, **43**(suppl.), S85–S94, DOI: **10.1093/ilar.43.suppl_1.s85**.

35 OECD.org, cited 2025 Mar 13, **https://www.oecd.org/en/publications/2013/07/test-no-236-fish-embryo-acute-toxicity-fet-test_g1g34036.html**.

36 P. Y. Muller and M. N. Milton, The determination and interpretation of the therapeutic index in drug development, *Nat. Rev. Drug Discov.*, 2012, **11**(10), 751–761, DOI: **10.1038/nrd3801**.

37 R. Palmeira-de-Oliveira, R. M. Machado, J. Martinez-de-Oliveira and A. Palmeira-de-Oliveira, Testing vaginal irritation with the Hen's Egg Test-Chorioallantoic Membrane assay, *ALTEX*, 2018, **35**(4), 495–503, DOI: **10.14573/altex.1710091**.

38 Nih.gov, cited 2025 Mar 13, **https://ntp.niehs.nih.gov/sites/default/files/iccvam/docs/protocols/ivocular-hetcam.pdf**.

39 OECD, Test No. 428: Skin Absorption: In Vitro Method, *OECD Guidelines for the Testing of Chemicals, Section 4*, OECD Publishing, Paris, 2004, DOI: **10.1787/9789264071087-en**.

40 Method SA, in OECD guideline for the testing of chemicals, Nih.gov, cited 2025 Mar 13, **https://ntp.niehs.nih.gov/sites/default/files/iccvam/suppdocs/feddocs/oecd/oecdtg428-508.pdf**.

41 D. Kaur and S. Chate, Study of antibiotic resistance pattern in methicillin resistant staphylococcus aureus with special reference to newer antibiotic, *J. Global Infect. Dis.*, 2015, **7**(2), 78, DOI: **10.4103/0974-777x.157245**.

42 Z. Pang, R. Raudonis, B. R. Glick, T.-J. Lin and Z. Cheng, Antibiotic resistance in Pseudomonas aeruginosa: mechanisms and alternative therapeutic strategies, *Biotechnol. Adv.*, 2019, **37**(1), 177–192, DOI: **10.1016/j.biotechadv.2018.11.013**.

43 Y. Li, S. Kumar, L. Zhang and H. Wu, Klebsiella pneumonia and its antibiotic resistance: a bibliometric analysis, *BioMed Res. Int.*, 2022, **2022**, 1–10, DOI: **10.1155/2022/1668789**.

44 M. A. A. Khalek, A. M. Abdelhameed and S. A. A. Gaber, The use of photoactive polymeric nanoparticles and nanofibers to generate a photodynamic-mediated antimicrobial effect, with a special emphasis on chronic wounds, *Pharmaceutics*, 2024, **16**(2), 229, DOI: **10.3390/pharmaceutics16020229**.

45 Y. Zhou, C. Jin, Y. Li and W. Shen, Dynamic behavior of metal nanoparticles for catalysis, *Nano Today*, 2018, **20**, 101–120, DOI: **10.1016/j.nantod.2018.04.005**.

46 T. Q. d. M. Bittencourt, T. P. Santos, P. E. d. S. Bastos, M. J. A. A. L. Amorim, S. d. S. Gomes, Y. M. L. d. Albuquerque and et al., A nanotoxicological approach to the effects of metformin and sodium metavanadate co-encapsulated in polycaprolactone nanoparticles under the biological parameters of zebrafish (Danio rerio), *Arch. Curr. Res. Int.*, 2024, **24**(12), 174–184, DOI: **10.9734/acri/2024/v24i121007**.

47 C. M. Carbaugh, W. H. van der Schalie and M. W. Widder, High throughput embryonic zebrafish test with automated dechorionation to evaluate nanomaterial toxicity, *PLoS One*, 2022, **17**(9), e0274011, DOI: **10.1371/journal.pone.0274011**.

48 M. I. Ortiz-Román, I. M. Casiano-Muñiz and F. R. Román-Velázquez, Ecotoxicological effects of TiO2 P25 nanoparticles aqueous suspensions on zebrafish (Danio rerio) eleutheroembryos, *Nanomaterials*, 2024, **14**(4), 373, DOI: **10.3390/nano14040373**.

49 S. S. Smail, Ex vivo irritation evaluation of a novel Brimonidine nanoemulsion using the hen's egg test on chorioallantoic membrane (HET-CAM), *Cureus*, 2024, **16**(8), e68280, DOI: **10.7759/cureus.68280**.

50 R. Yadav and N. R. Pandey, A Cytotoxic evaluation by HET CAM on Chick embryo and Antimicrobial assay of Silver Nanoparticles synthesized from Green Tea Extract, *Ymer*, 2022, **21**(6), 921–929, DOI: **10.37896/ymer21.06/91**.

51 A. Öztürk, T. Çevikelli, E. K. Tilki, U. M. Güven and H. T. Kıyan, Ketorolac Tromethamine Loaded Nano-Spray Dried Nanoparticles: Preparation, Characterization, Cell Viability, COL1A1 Gene Simulation and Determination of Anti-inflammatory Activity by In Vivo HET-CAM Assay, *Curr. Drug Delivery*, 2023, **20**(6), 830–840, DOI: **10.2174/1567201820666230125144133**.

52 I. Pulsoni, M. Lubda, M. Aiello, A. Fedi, M. Marzagalli, J. von Hagen, *et al.*, Comparison between Franz Diffusion Cell and a novel micro-physiological system for in vitro penetration assay using different skin models, *SLAS Technol.*, 2022, **27**(3), 161–171, DOI: **10.1016/j.slast.2021.12.006**.

53 M. Kumar, A. Sharma, S. Mahmood, A. Thakur, M. A. Mirza and A. Bhatia, Franz diffusion cell and its implication in skin permeation studies, *J. Dispers. Sci. Technol.*, 2024, **45**(5), 943–956, DOI: **10.1080/01932691.2023.2188923**.

54 F. Iliopoulos, P. J. Caspers, G. J. Puppels and M. E. Lane, Franz cell diffusion testing and quantitative Confocal Raman Spectroscopy: In vitro-in vivo correlation, *Pharmaceutics*, 2020, **12**(9), 887, DOI: **10.3390/pharmaceutics12090887**.